ECT Studies of the Choking Phenomenon in a Gas–Solid Circulating Fluidized Bed

Bing Du, W. Warsito, and Liang-Shih Fan
Dept. of Chemical Engineering, The Ohio State University, Columbus, OH 43210

DOI 10.1002/aic.10168
Published online in Wiley InterScience (www.interscience.wiley.com).

Choking is commonly defined as a phenomenon where a sudden change in the solids holdup occurs in a gas–solid fluidization system. In this study, the electrical capacitance tomography (ECT) based on the neural network multicriteria optimization image reconstruction technique (NNMOIRT), developed by this research group, is used to probe the mechanism of choking formation by examining a real-time, quasi-3D cross-sectional flow structure of a circulating fluidized bed riser. The particles used are FCC catalysts. The ECT with NN-MOIRT reveals a double solids-ring flow structure and the presence of particle blobs at the center of the bed in the circulating fluidized bed (CFB) riser. This flow structure, when it is present at the entrance region of the riser, undergoes a distinct variation during the choking transition when the gas velocity is below the transport velocity U_{tr}, but does not undergo a distinct variation when the gas velocity is above U_{tr}. This flow structure, when it is present at the upper region of the riser, however, does not vary distinctly at any gas velocity. Such flow structure variations are not appreciably affected by the solids feeding patterns with or without a gas or solids distributor, or by the gas humidity. For the low gas velocities ($<U_{tr}$), the borescope measurement indicates that the solids concentration in the particle blob and the blob size all increase as the solids circulation rate increases. The disintegration of the enlarged blobs or blob jets and the collapse of the solids suspension characterize the mechanics of the initiation of the choking transition to the dense-phase fluidization regime attributed to solids suspension instability. © 2004 American Institute of Chemical Engineers *AIChE J,* 50: 1386–1406, 2004
Keywords: choking, circulating fluidized bed, electrical capacitance tomography, fast fluidization, transport velocity

Introduction

The term "choking" commonly refers to a gas–solid fluidization phenomenon in which a small change in gas or solids flow rate prompts a large change in the hydrodynamic behavior such as the pressure drop or solids holdup during the gas–solid flow. A fundamental understanding of the mechanism of choking phenomenon is of great importance to the operation of circulating fluidized bed (CFB) reactors and pneumatic transport systems. Considerable efforts have been made in probing the choking phenomenon in gas–solid circulating fluidized beds. Nevertheless, the fundamental nature of the occurrence of choking, the choking transition from dilute fluidization to dense fluidization, and its underlying mechanism still remain unclear.

Several reviews on the choking phenomenon and flow regime transition in vertical pneumatic conveying systems have been presented (Bi and Grace, 1995; Bi et al., 1993; Xu et al., 2001). Bi et al. (1993) classified choking into three types. Type A choking, or *accumulative* choking, refers to the occurrence of an accumulation of particles at the bottom of the CFB riser, characterized by an abrupt change in voidage or pressure drop (Matsen, 1982; Yerushalmi and Cankurt, 1979). Type A choking marks the regime transition between pneumatic transport

Correspondence concerning this article should be addressed to L.-S. Fan at fan.1@osu.edu.

© 2004 American Institute of Chemical Engineers

and fast fluidization. Type B choking, or so-called *blower-standpipe–induced* choking, is caused by the operational characteristics of gas compression devices such as the gas blowers or compressors, or by solids feeding related devices such as standpipes or L-valves. Type C choking, or *classical* choking, is represented by the formation of slugs. Type C choking marks the regime transition between fast fluidization and slugging fluidization when there is sufficient blower pressure and solids feeding. Xu et al. (2001) observed that Type A choking is initiated by the collapse of the dilute suspension. They reported that the differential pressure drop and the corresponding solids concentration at the choking point are independent of the gas velocity and the riser diameter, but vary with particle properties (diameter and density). From their experimental results and data in the literature, they reported a correlation for the saturation carrying capacity as a function of the gas velocity, bed diameter, and particle properties. The review by Wang and Rhodes (2002) recently disputed the use of choking as a criterion to describe the boundaries at the onset or the end of fast fluidization to be coincidental. They defined choking as the point when all solids cannot be entrained by the gas, as given by Zenz and Othmer (1960). They indicated that choking and fast fluidization are the same process but different types of transition from dilute to dense-phase fluidization under different conditions. Therefore, choking and regime transition, either from dilute transport to fast fluidization or from fast fluidization to dense fluidization, are a separate matter.

The choking transition has been predicted primarily based on pure-empirical or semi-empirical correlations. The progress on the comprehensive mechanistic modeling of the choking transition, however, has been hampered because of the lack of the fundamental understanding of the choking phenomenon. Various assumptions were made in modeling efforts. For example, by assuming the voidage and the slip velocity at the onset of choking to be 0.97 and the terminal velocity of a single particle, respectively, Leung et al. (1971) derived a correlation that predicts the choking velocity of solids in vertical pneumatic systems. Capes and Nakamura (1973), on the other hand, noted that the slip velocity at the onset of choking could be greater than the terminal velocity of a single particle because of the particle–wall friction and particle recirculation effects. They stated that choking occurs when the particles begin to recirculate. They noted, then, that the choking data were difficult to obtain accurately because the occurrence of the choking spans over a range of gas and solids velocities in a vertical pneumatic system. Using the same assumption concerning the slip velocity at choking as that of Leung et al. (1971), Yang (1975) considered the choking point in a CFB riser to be reached when the solids friction factor was equal to 0.01. Yang (1983) further modeled the choking point by using a correlation to describe the solids friction factor. Yang (1983) also developed a semi-empirical correlation by applying a new mechanistic model based on cluster formation and continuity wave theory. Matsen (1982) attributed the initiation of choking in vertical pneumatic systems to the formation of clusters. They derived a numerical expression to describe the relationship between the slip velocity and the terminal velocity of single particles at different solids concentration. Day et al. (1990) introduced a parameter $\gamma(\epsilon)$, as follows:

$$\gamma(\varepsilon) = \frac{\rho_p U_p^2}{(1-\varepsilon)^2} - \frac{\rho_g U_g^2}{\varepsilon^2} \tag{1}$$

and assumed that choking happened when γ at the inlet to the CFB riser was equal to 0. There is no physical meaning for this parameter.

Most studies with regard to the choking phenomenon in vertical pneumatic conveying systems involve pressure drop measurements. The solids holdup is commonly obtained from the pressure drop data by assuming solids to be in complete suspension without solids acceleration. The global property for the solids holdup obtained in this manner does not reveal the flow structure in the riser system. The local solids holdup can be measured using the optical-fiber probe or the capacitance probe. The probe interferes with the main flow and induces measurement errors especially in the dilute pneumatic transport regime. Little information is available concerning the flow structure and its dynamic behavior, particularly during the choking transition. The lack of accurate, instantaneous, and simultaneous techniques for measurement along the bed cross section prevents a precise description of the flow structure underlining the choking condition.

Process tomography is an important nonintrusive technique that uses remote sensors to obtain time-averaged or real-time field images. A number of tomography techniques, such as X-ray, γ-ray, optical, ultrasonic, electrical, and nuclear magnetic resonance imaging, have been developed and applied to study complex multiphase phenomena (Beck and Williams, 1996; George et al., 2000; Kumar et al., 1997; Rowe, 1971; Seville et al., 1986; Warsito et al., 1999). Electrical capacitance tomography (ECT) is one of a handful of real-time tomography techniques and has been applied recently to three-phase flow imaging (Warsito and Fan, 2001a). ECT has also been applied to other solid flow systems, including standpipe flow, bubbling and turbulent fluidized beds, circulating fluidized beds, pneumatic conveying, and cyclone diplegs (Du et al., 2002, 2003; Dyakowski et al., 1997, 2000; Makkawi and Wright, 2002a, 2002b; Malcus and Pugsley, 2001; Malcus et al., 2000; Smolders et al., 2001; Yang and Liu, 2000). The crux for the accurate application of the ECT or any other tomography techniques is the robustness of the image reconstruction technique used in resolving the "inverse" tomography imaging problem (Warsito and Fan, 2001b).

Objectives of This Work

The behavior of the differential pressure drop variation is usually used to identify the collapse of dilute suspension or the initiation of choking in a vertical CFB riser. Figure 1 shows the variation of differential pressure drop with the solids circulation rate at different gas velocities with FCC particles. It is observed that choking occurs first at the bottom of the riser (that is, the entrance or the acceleration region of the riser). Measurements thus focus on the location in this region. For the purposes of comparison, measurements are also made at the upper region of the riser. Measurements at the gas velocities that are less than the transport velocity ($<U_{tr}$) and greater than the transport velocity ($>U_{tr}$) are also made to discern the difference in flow structure variation in flow regime transition or choking transition. As shown in Figure 1, at a low gas

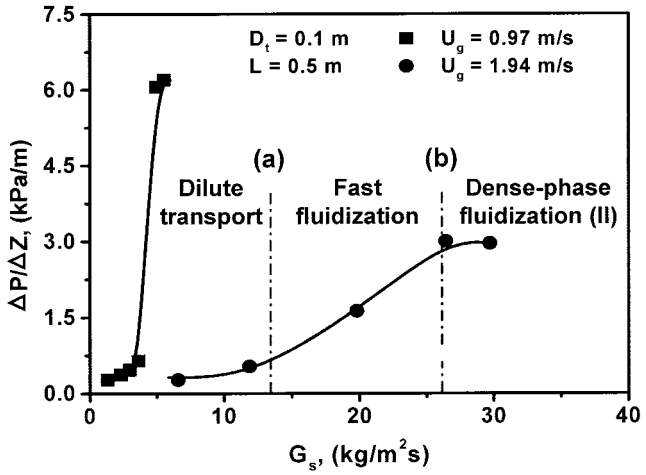

Figure 1. Variation of pressure gradients with solids circulation rate.

velocity ($<U_{tr}$) there is a sharp increase in pressure drop with increasing solids circulation rates, whereas at a high gas velocity ($>U_{tr}$) the pressure drop increases gradually with solids circulation rates. This is similar to the results reported by Yerushalmi and Cankurt (1979) and Xu et al. (2001). Yerushalmi and Cankurt (1979) then defined the regime transition between turbulent fluidization and fast fluidization based on U_{tr}. From these studies, one could deduce that if choking is defined as the sharp increase in the pressure drop, either with increasing solids circulation rate at a given gas velocity or with decreasing gas velocity at a given solids circulation rate, it will occur only when the gas velocity is lower than U_{tr} or the solids circulation rate is smaller than the transport solids circulation rate $G_{s,tr}$. When the gas velocity or the solids circulation rate is larger than U_{tr} or $G_{s,tr}$, the pressure drop increases and the suspension becomes gradually denser with increasing solids circulation rate or decreasing gas velocity. Thus, this behavior would not be commensurate with the fundamental definition of choking. Type C choking reported by Bi et al. (1993), on the other hand, would be commensurate with the fundamental definition of choking. Clearly, the issue of choking still merits further examination, particularly from the perspective of the fundamental mechanism of choking formation and its flow structure variation.

The dilute transport regime is characterized by a homogeneous flow structure with uniform solids holdup distribution in both axial and radial directions, whereas the fast fluidization regime is characterized by the heterogeneous flow structure with a dense region in the lower part and dilute region in the upper part of the riser. The dense region includes a dilute core region and a dense annular region, whereas the dilute region at the upper part of the riser is relatively homogeneous. However, examining the existing experimental data on radial solids holdup distribution (Neri and Gidaspow, 2000; Parssinen and Zhu, 2001; Wei et al., 1998; Wiesendorf and Werther, 2000; Zheng et al., 2001) obtained by optical-fiber probe, capacitance probe, or X-ray densitometer, as shown closely in Figure 2, the solids holdup is far from monotony in its increase with an increase in the radial distance from the center to the wall in the riser. Such a radial solids holdup profile appears to be overlooked by any computational fluid dynamic models (for example, Neri and Gidaspow, 2000; Zheng et al., 2001) in their prediction of the riser hydrodynamics. Although the solids holdup is generally lower in the core region and higher near the wall, these radial profiles signify a uniform solids holdup structure presence in the CFB riser. Because of the lack of a reliable experimental technique for accurate, real-time image of gas–solid flow or multiphase flow, the qualitative and quantitative information regarding microscopic and macroscopic flow structure of the gas–solid fluidization is inadequately known. The pressure drop can provide the overall information only for the flow behavior of a CFB riser. The intrusive probe measurement would provide point information, but it does not offer overall field dynamic information. The effect is even more remarkable for the dilute system. Therefore, the second objective of this work is to characterize the dynamic behavior of a gas–solid circulating fluidized bed using the electrical capacitance tomography (ECT) and ECT velocimetry adopted with a newly developed image reconstruction technique. With these measurements, the detailed dynamic flow structure of the gas–solid riser flow can be quantified. The specific focus of this study is thus to reveal the flow structure pertaining to choking and to present a perspective of the regime transition in relation to choking from the flow structure variation point of view.

Experimental Studies

Setup

The schematic diagram of the circulating fluidized bed used in this study is shown in Figure 3. The experimental unit consists of a 0.1-m ID riser with a height of 6.32 m, a separator and secondary cyclone system, a large volume particle storage hopper, and an L-valve. The entire system is made of Plexiglas except the steel particle separator. Particles are carried upward in the riser and exit at the top through a right-angled bend into a horizontal tube connected to the separator and secondary cyclone where the particles are separated from the gas. Subse-

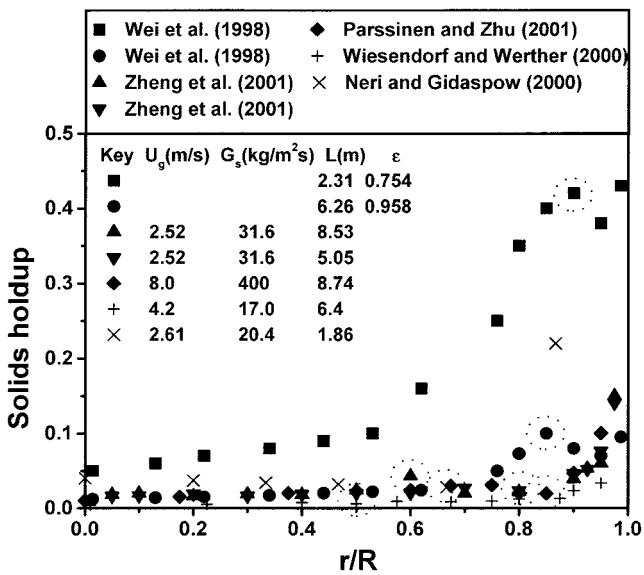

Figure 2. Reported experimental results obtained by the probe measurement.

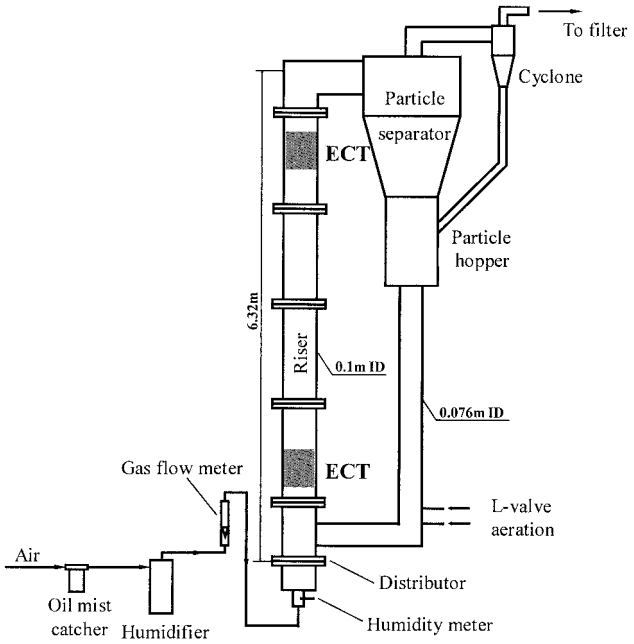

Figure 3. Circulating fluidized bed.

quently, the particles are fed back to the bottom of the riser through the nonmechanical L-valve. The solids circulation rate, which is controlled by adjusting the air aeration rate at the injection points of the L-valve, is measured by timing the falling distance of tracer particles in the standpipe. The compressed air is introduced into the riser through an oil filter, humidifier, pressure manometer, and flow meter. The air humidity is controlled by the water level and water temperature in the humidifier. The relative humidity and temperature are measured by means of a humidity probe inserted into the air stream. The superficial gas velocity is measured by the flow meter adjusted by the temperature and pressure of the airflow.

A differential pressure transducer is installed to measure the pressure drop and the overall voidage of the fluidized bed. The local solids holdup is measured by the optical-fiber probe (Du et al., 2003). The fluidized particles used in this study are FCC catalysts with a mean diameter of 60 μm and particle density of 1400 kg/m^3.

Electrical capacitance tomography

The electrical capacitance tomography (ECT) system, consisting of a capacitance sensor, data acquisition system, and computer system for image reconstruction, interpretation, and display, is illustrated in Figure 4. The capacitance sensor array consists of a twin-plane sensor (plane 1 and plane 2) using 12 electrodes for each plane attached to the outside of the column wall. The length of each electrode is 0.05 m. Two 0.05-m-long guard sensor planes are located above and below the measuring sensor planes to adjust the electrical field within the sensoring area. There are 66 combinations of independent capacitance measurements between electrode pairs from 12 electrodes. The data acquisition system manufactured by Process Tomography Ltd. (UK) is used for capturing the ECT images at 100 frames/s. A novel reconstruction algorithm based on an analog neural network multicriteria optimization image reconstruction technique (NN-MOIRT) developed earlier by the authors (Warsito and Fan, 2001b) is applied to achieve the image reconstruction. The technique transforms capacitance data into cross-sectional images of the gas–solids two-phase flow at 32×32 pixels per image. A parallel capacitance model is used to convert the permittivity pixel value to the solids holdup value. The technique has been verified and applied to the study of the flow dynamics of gas–solid fluidized beds (Du et al., 2002, 2003), gas–liquid bubble columns, and three-phase fluidized beds (Warsito and Fan, 2001a, 2003a). Because of the accuracy of this algorithm, the local dynamic properties of complex two-phase or three-phase media can be quantified with confidence. The details of this technique, the image reconstruction algorithm, and its comparisons with other algorithms are described elsewhere (Warsito and Fan, 2001b). The output signal of the ECT measurement spans from zero to one. Zero is set for the empty bed and one is set for the packed bed. The real solids holdup in the measuring area is the output signals of the ECT multiplied by the solids holdup of the packed bed. Details on the solids holdup measurement in a gas–solid fluidized bed are described in Du et al. (2003).

A tomography image velocimetry (TIV), developed by the authors earlier (Warsito and Fan, 2003b) based on cross-correlation of quasi-3D tomography images in two planes, is used to calculate the particle aggregate or blob velocity in the gas–solid circulating fluidized bed. Two cross-correlation domains in one plane (that is, center region and near-wall region) are determined to calculate the particle velocities in the center and near-wall regions of the column. Details of the velocimetry technique are described elsewhere (Warsito and Fan, 2003b).

Borescope

A borescope system as well as a high-speed video camera is used to visualize the internal flow structure, especially the behavior of the particle aggregation in the circulating fluidized bed. The diagram of this system is shown in Figure 5. The light from the source is delivered into the bed by optical fiber. Simultaneously, the light reflected by the particles in the bed is captured by the optical fiber and transferred to the borescope, where the reflected light is transformed to the visualized images. These images are then recorded by the high-speed video

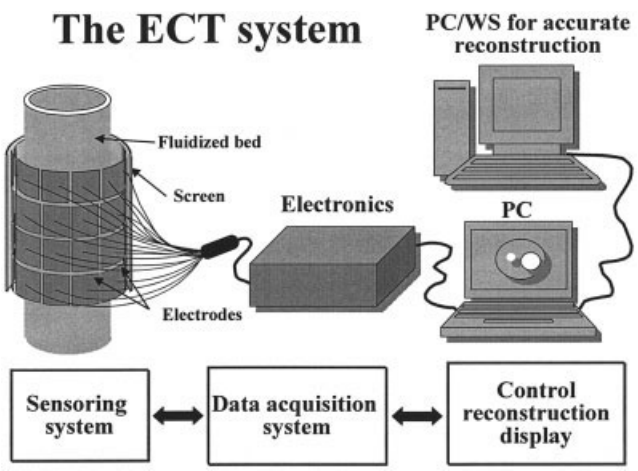

Figure 4. ECT system.

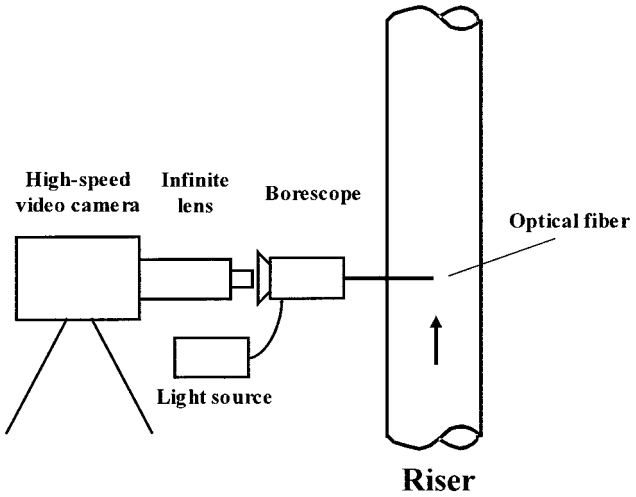

Figure 5. Borescope system.

camera by means of an infinite lens. The diameter of the optical-fiber probe is about 2 mm. To avoid the attachment of particles around the tip of the optical-fiber probe, ascribed to the electrostatic effect, purging air is introduced to blow out the attached particles. The flow interference resulting from the purging air can be ignored because the flow rate of the purging air is very low.

Results and Discussion

For a gas–solid circulation system, the fluidization regimes are confined by both the superficial gas velocity and the solids circulation rate, as shown in Figure 6. The solid line in the figure representing the boundary between the dense-phase fluidization regime and the fast fluidization regime U_{tf} was correlated by Bi and Fan (1991):

$$\frac{U_{tf}}{\sqrt{gd_p}} = 39.8\left(\frac{G_s}{\rho_g U_{tf}}\right)^{0.311} \mathrm{Re}_t^{-0.078} \tag{2}$$

The dash line—the boundary between the fast fluidization regime and the dilute transport regime (U_{fd})—is described as follows (Bi and Fan, 1991):

$$\frac{U_{fd}}{\sqrt{gd_p}} = 21.6\left(\frac{G_s}{\rho_g U_{fd}}\right)^{0.542} \mathrm{Ar}^{0.105} \tag{3}$$

The point from the intersection of these two lines corresponds to the transport gas velocity U_{tr} and the transport solids circulation rate $G_{s,tr}$. The fast fluidization regime is confined between these two lines at gas velocities greater than U_{tr}. The dilute transport regime and the dense-phase fluidization regime are located below U_{fd} and above U_{tf}, respectively. To study the flow behavior of the vertical gas–solid circulating fluidized bed systematically, experiments are carried out for three cases with the gas velocities lower than U_{tr}, about equal to U_{tr}, and higher than U_{tr}. The specific flow conditions are indicated by star symbols given in Figure 6. These flow conditions cover all the essential fluidization regimes.

The solids holdup distributions in real time (with a time interval of 0.02 s), in planes 1 and 2 under different operation conditions, are shown in Figure 7. The color bar variation from blue to red at the bottom right of the figure represents the variation of solids concentration from low to high (0 to 0.1 for this figure). Figure 7a shows the solids holdup distribution at a solids circulation rate of 1.32 kg m^{-2} s^{-1} and a gas velocity of 0.97 m/s ($<U_{tr}$). There are two clear solids rings across the bed: one is surrounding the gas core at the center of the bed and the other is near the wall. Between these two solids rings there is a gas ring. With time variation, this double solids-ring flow structure does not exhibit a significant change, although the solids holdup in this flow structure may vary. Figure 7b shows the solids holdup distribution at a solids circulation rate of 11.9 kg m^{-2} s^{-1} and a gas velocity of 1.94 m/s ($>U_{tr}$). There are three regions across the bed: a solids core referring to the center core region of the bed with a higher solids concentration than its vicinity, a solids ring near the wall, and a gas ring between them. The shape and the solids concentration of the solids core are always varying with time. The flow structure is persistent. By comparing the solids holdup distributions in plane 1 and plane 2, it can be seen that the distribution patterns in the plane pairs are quite similar. Furthermore, the fact that the imaging plane is 0.05 m in length and is substantially shorter, compared to the entire riser length of 6.32 m, indicates that the effect of space averaging over the 5 cm length of the sensor electrode can be ignored and the images obtained by the ECT reconstruction can describe the real flow behavior in the bed cross section.

Dynamic behavior of a CFB at $U_g < U_{tr}$

By stacking 200 tomographic images obtained in 4 s from the same plane, a quasi-3D flow structure of a CFB riser can be displayed. Figure 8 shows the quasi-3D solids holdup distribution in plane 1 of the ECT at the lower part of the riser (0.5 m above the distributor) under different solids circulation rates at a lower gas velocity of 0.97 m/s. The images for each solids circulation rate from two sliced sections representing the solids holdup distribution in the X–Z and Y–Z planes are shown in the figures. There is a color bar under the two images in the X–Z and Y–Z planes for each solids circulation rate. Similarly,

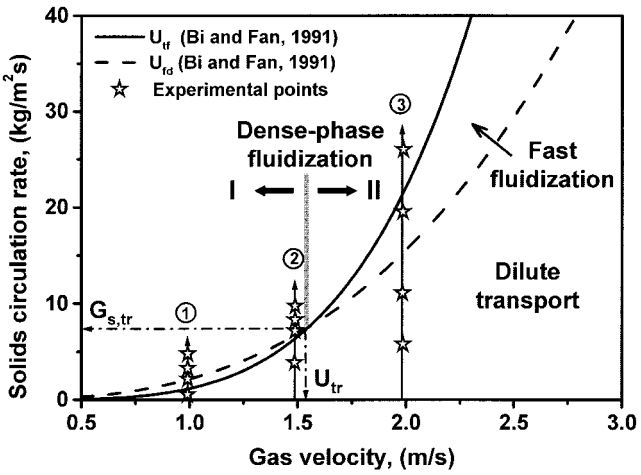

Figure 6. Experimental conditions based on the map of fluidization regimes.

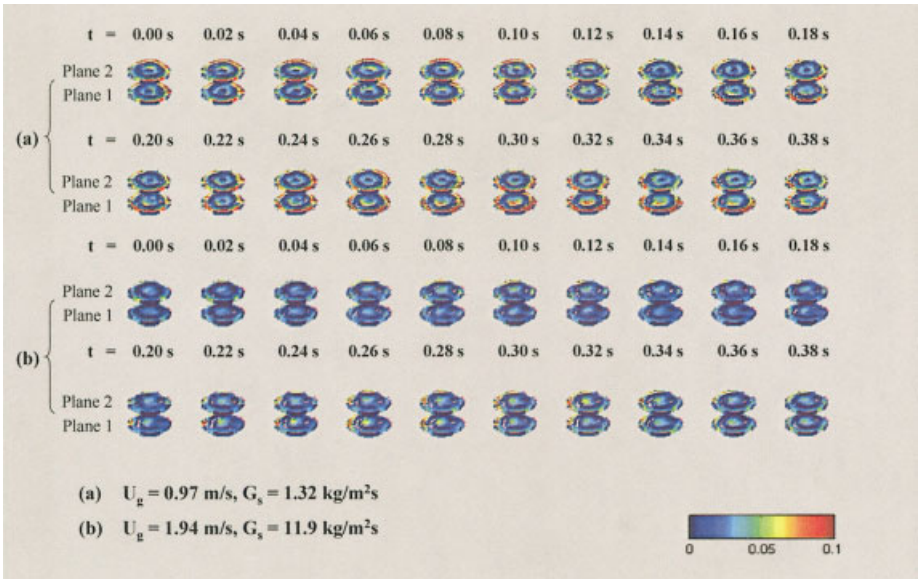

Figure 7. Real-time solids holdup distributions measured by ECT.

the blue area represents the low solids concentration. The red area represents the high solids concentration, which varies with the solids circulation rate to clearly reflect the flow structure in a riser. At a low solids circulation rate of 1.32 kg m^{-2} s^{-1}, the flow structure depicted in Figure 8a is different from earlier work noted above, that is, a uniform flow structure for the dilute transport regime and a core–annulus structure for the fast fluidization regime. The solids concentration is the highest near the wall region where a solids ring is formed over the riser cross section. These particles move downward from visual observation in the experiments. Transients in solids concentration variation reveal the presence of an inner region surrounding a transitory, small, and dilute gas core. Some particles in this inner region tend to aggregate to form blobs. The solids concentration of the blobs is comparable to that in the solids ring near the wall. The size, shape, and the concentration of blob vary significantly with the time. Between the inner region and the solids ring near the wall, there is a gas ring with very low solids holdup. It is also observed that particles interchange continuously between the inner region and the solids ring near the wall. With an increase in the solids circulation rate to 2.3 kg m^{-2} s^{-1}, the solids concentration distribution in the column, as shown in Figure 8b, increases compared to that in Figure 8a. There is a solids core observed at the center of the bed.

A persistent dilute gas ring is clearly observed between the solids core and the solids ring near the wall. The solids concentration in the solids ring near the wall is higher than that in the solids core region, and the difference between them is more

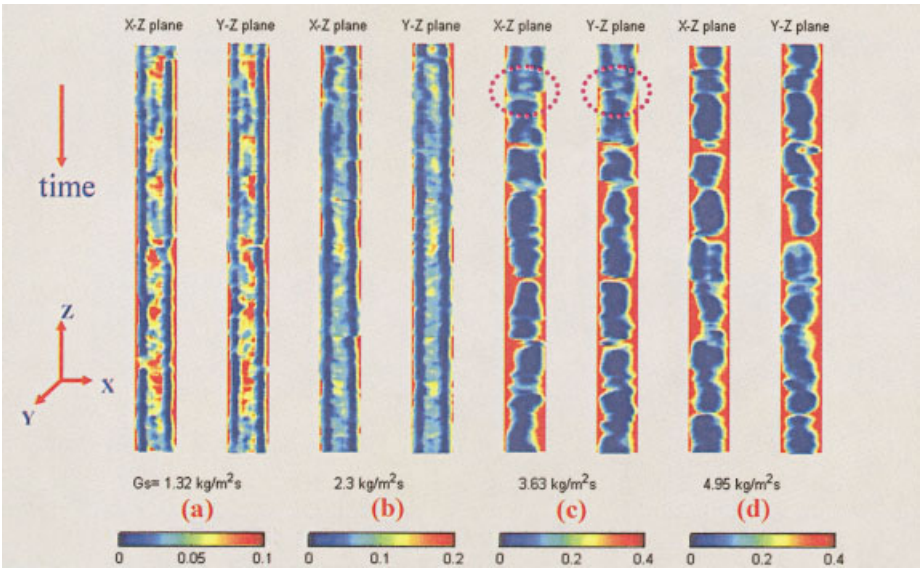

Figure 8. Quasi-3-D flow structures at lower part of a CFB riser at a gas velocity of 0.97 m/s.

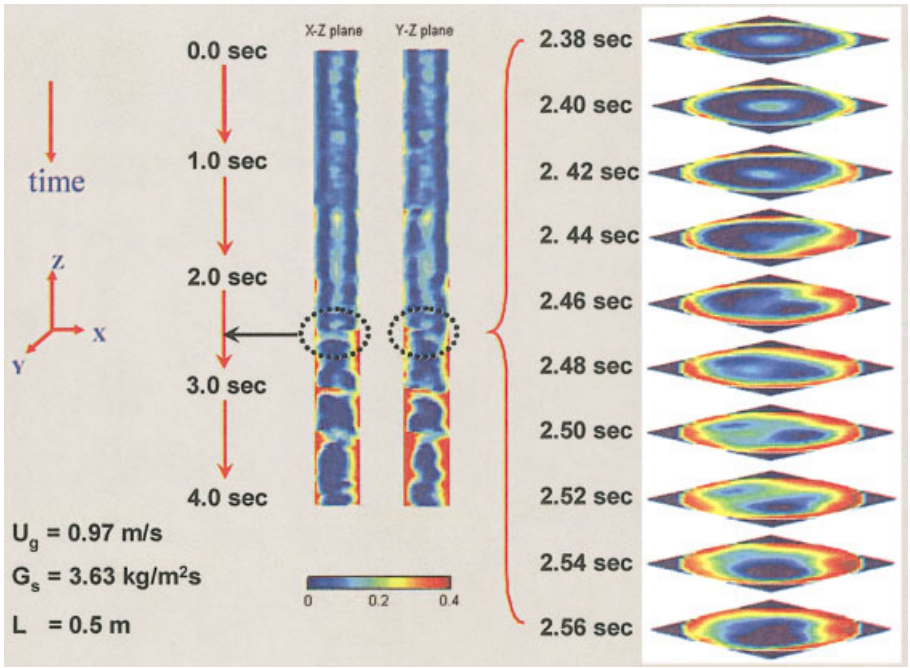

Figure 9. Choking transition with flow structure variation at $U_g < U_{tr}$.

remarkable compared to that for the lower solids circulation rate condition. A clear solids exchange occurs between the dense core and the solids ring through the dilute gas ring region. Under this solids circulation rate condition, solids tend to aggregate, and move upward as a blob at the center of the bed and downward as a cluster at the wall of the bed. The blobs may connect with each other forming the blob jets in the column, which is in the transient behavior between formation and breakage. When the solids circulation rate undergoes a step increase to 3.63 kg m^{-2} s^{-1}, the transient flow structure is shown in Figure 8c. The flow structure at the top of Figure 8c shows a comparable one, albeit denser, to that for Figure 8b. It is seen, however, that, after a short period, an abrupt, sharp variation of the flow structure takes place. The solids blobs disappear suddenly and all the particles move to the dense wall region with a large dilute gas core occurring in the central region.

This abrupt flow structure change marks the well-known choking transition to dense-phase fluidization. To examine this choking transition closely, a detailed flow structure variation is

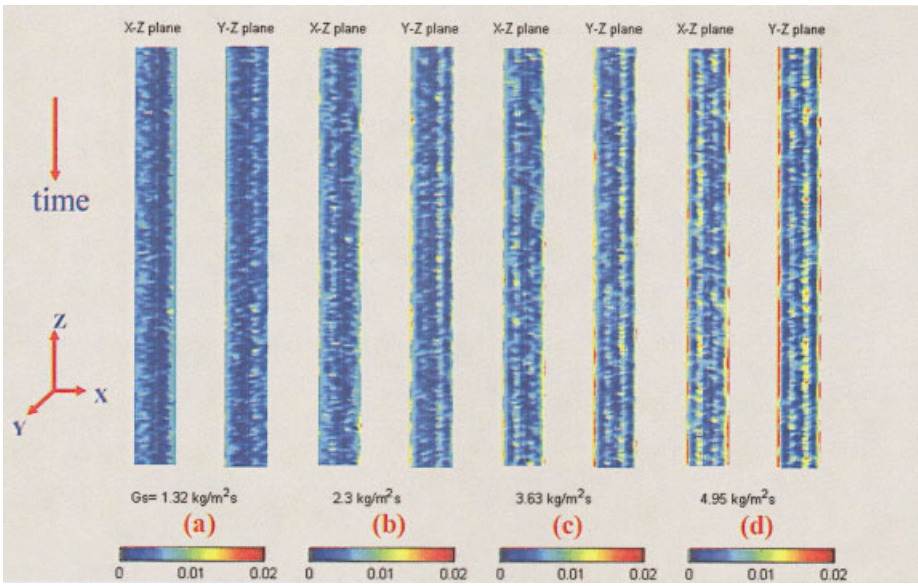

Figure 10. Quasi-3-D flow structures at upper part of a CFB riser at a gas velocity of 0.97 m/s.

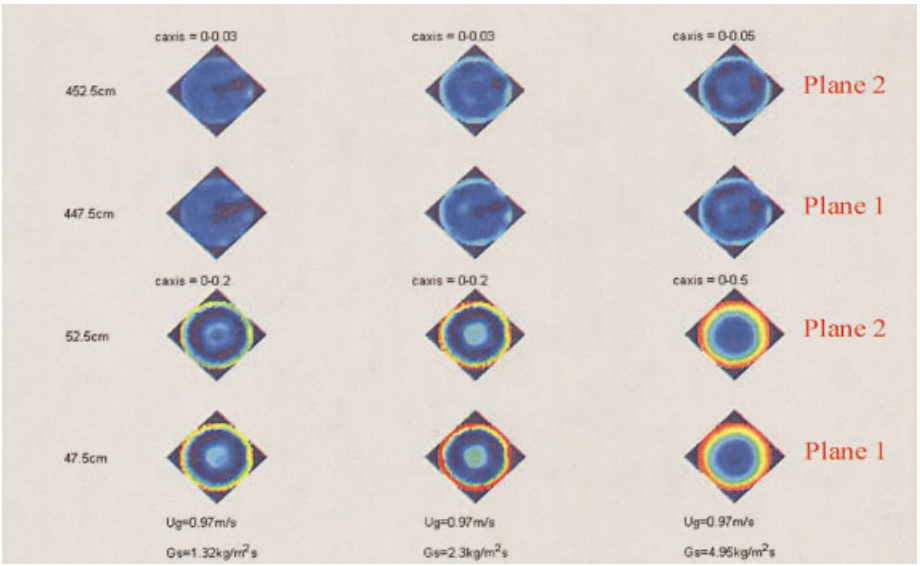

Figure 11. Time averaged cross-sectional solids holdup distributions at a gas velocity of 0.97 m/s.

shown in Figure 9. The large images at the right side of the figure illustrate the choking transition with flow structure variation. At 2.4 s after the step change of the solids circulation rate, the solids concentration in the solids core is about 0.15 and that in the solids ring near the wall is about 0.25. At 2.42 s, particles in the solids core region begin to move to the wall region. Subsequently, particles are in the dynamic process moving between the core region and the wall region in the bed. This process is noted as the choking transition. The total process lasts 0.12 s until the new flow structure with a dilute core region and a dense wall region is formed. After the transition, the solids concentration in the wall region increases sharply to about 0.4, and the size of the wall region also significantly increases. The solids core region is replaced by gas core region in this transition. The flow structure does not change much as the solids circulation rate further increases to 4.95 kg m^{-2} s^{-1}, as shown in Figure 8d. The gas core with varied shapes rises in the center of the bed and rocks between the sides of the column wall. Under the solids circulation rate of 4.95 ckg m^{-2} s^{-1}, the size of the gas core becomes smaller and more particles are present at the center of the bed. The particles at the center are carried upward by the violent gas movement and then move downward at the wall. It is also noted that the flow behavior after the choking point in the solids circulating system is similar to that for the solids-batch dense-phase fluidization system. There are a number of correlations accounting for the gas velocity and the solids circulation rate at the choking point proposed in the literature. The calculated results are different from different authors. Under this gas velocity ($<U_{tr}$), the solids circulation rate calculated by the correlations of Bi and Fan (1991), Xu et al. (2001), and Yousfi and Gau (1974) are most consistent with the experimental result obtained in this study.

Figure 10 shows the solids holdup distribution at the upper part of the riser (4.5 m above the distributor) under different solids circulation rate at the gas velocity of 0.97 m/s. The solids circulation rates used are the same as those for Figure 9. The color bar is given at the bottom of the figure. It can be seen that the solids holdup in the upper part of the riser is much lower than that in the lower part. At a lower solids circulation rate of 1.32 kg m^{-2} s^{-1}, the solids holdup is much less than 0.01. Although the solids holdup near the wall is higher than that in the core region (as shown in Figure 10a), the solids concentration difference in the radial direction is not significant. With an increase in the solids circulation rate to 2.3 kg m^{-2} s^{-1}, the downward particles appear near the wall. Two regions with high solids concentration and very low solids concentration are present between the dense wall and dilute core regions, as shown in Figure 10b. Compared to Figure 9, the central region with high solids concentration shown at the lower part of the riser is seen to expand outward at the upper part of the riser. The dilute core region thus becomes larger. Relatively more particles are present in the dilute region between the two dense regions at the center and near the wall of the bed, reflecting the frequent exchange of particles between these two dense regions. When the solids circulation rate increases to 3.63 kg m^{-2} s^{-1} (as shown in Figure 10c), corresponding to the choking transition point in the lower part of riser at the gas velocity of 0.97 m/s, the solids holdup in each region across the bed increases, particularly in the wall region. There is no change in the flow structure, however, in the upper region of the riser under this condition. The particle interchange between the two dense regions is also enhanced. Figure 10d shows the solids holdup distribution at a solids circulation rate of 4.95 kg m^{-2} s^{-1}, corresponding to the condition after the choking transition in the lower part of riser. The solids holdup in each region increases with significant solids exchange between the two dense regions. Therefore, at a lower gas velocity ($<U_{tr}$), the general flow structure at the upper part of the riser is unchanged irrespective of the solids circulation rate, although the solids holdup in each region across the bed increases with increasing solids circulation rate.

Figure 11 shows the 20-s time averaged cross-sectional solids holdup distribution at different solids circulation rates in planes 1 and 2 at both the lower part and upper part of the riser. The "caxis" in the figure represents the magnitude variation of

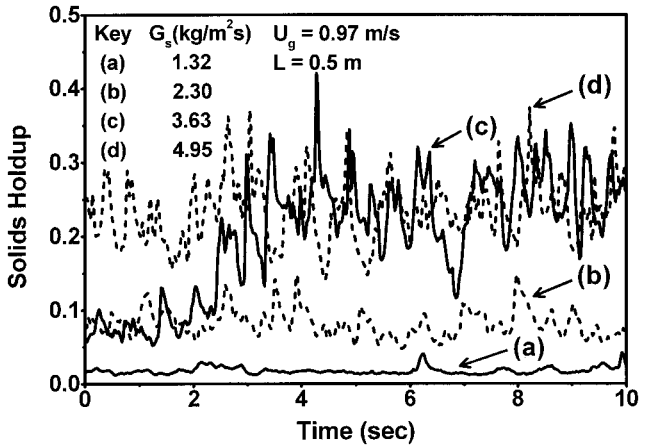

Figure 12. Transient solids holdup distributions at lower part of a riser at a gas velocity of 0.97 m/s.

the solids holdup and their corresponding colors in the image indicator spanning from blue (lowest) to red (highest). Based on the definition of choking given above, the first two figures show the time-averaged flow behavior before the choking transition and the third one shows the time-averaged flow behavior after the choking transition. The solids holdup in the lower part is much higher than that in the upper part. Regarding either the lower part or the upper part of the riser, the solids holdup in plane 1 is higher than that in plane 2. The time-averaged cross-sectional solids holdup exhibits a radial symmetric distribution under all operation conditions. The solids holdup increases with increasing solids circulation rate. At the lower part of the riser, especially, there is a significant increase in the solids holdup after the choking transition, reflected by the large area of red color in the image and the high value in the color axis. At the lower part of the riser, the images in the figure clearly depict the flow structure in the different regimes. At the solids circulation rate of 1.32 kg m^{-2} s^{-1}, the bed exhibits the double solids-ring flow structure, more remarkable in plane 2. One solids ring is located at the center region of the bed covering a dilute core and the other is near the wall. There is a very dilute gas ring between these two solids rings. With the increase of the solids circulation rate to the transition regime before choking, the solids ring at the center combines with the dilute core into the dense solids core region. The solids concentration in both the solids core region and the solids ring near the wall greatly increase. After the choking transition, the solids core disappears and only two regions exist, one dilute core region and one dense wall region. At the upper part of the riser, the solids holdup is almost unvaried along the radial direction at the lowest solids circulation rate. The other two situations show double solids-ring flow structure. At the solids circulation rate of 2.3 kg m^{-2} s^{-1} before choking, there are numerous particles present in the dilute region between the two rings, making the boundaries between these regions indistinct. It also indicates that the particles exchange frequently at the upper part of the riser and the bed tends to behave as a uniform structure. However, when the solids circulation rate increases to 4.95 kg m^{-2} s^{-1} after the choking transition, the boundaries are clear and the double solids-ring structure is more persistent. Compared to the double solids-ring structure at the lower part of the riser, the areas of the dilute core and the ring near the wall are almost the same but the ring in the center region becomes thicker at the upper part of the riser. It can be concluded that the double solids-ring structure is robust in a dilute CFB riser. The ring in the center region gradually expands outward to the wall along the axial positions.

To illustrate the choking transition objectively, the transient cross-sectional solids holdup distributions measured by the ECT at the lower part of the riser under different solids circulation rates are shown in Figure 12. At a lower solids circulation rate, as shown in line (a), the solids holdup is very low and the fluctuation is also very small, reflecting a uniform flow or pluglike flow in the bed. With an increase in the solids circulation rate, both the solids holdup and the fluctuation increase, as shown in line (b). When the solids circulation rate further increases to 3.63 kg m^{-2} s^{-1}, there is a sharp change of the solids holdup from less than 0.1 to around 0.27, which is noted as choking in the literature (Bi et al., 1993; Satija et al., 1985). Furthermore, the fluctuation of the solids holdup distribution substantially increases, reflecting a turbulent flow behavior

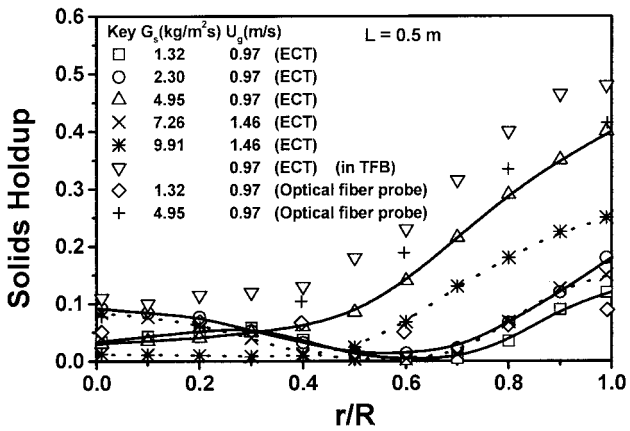

(a) Lower part of a riser

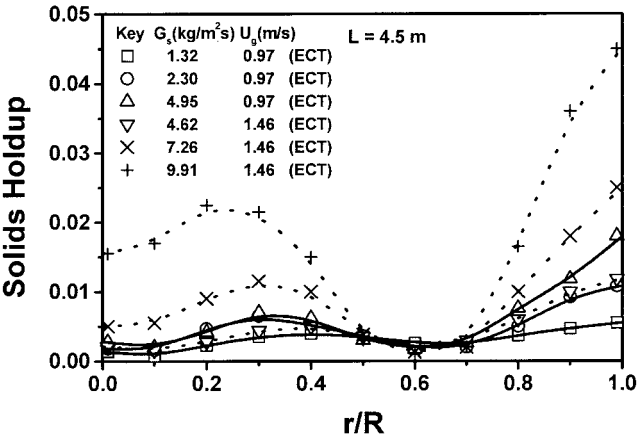

(b) Upper part of a riser

Figure 13. Radial solids holdup distribution at $U_g < U_{tr}$.

induced by the violent gas movement. Because the pressure drop is represented by the solids holdup when the solids are fully suspended, this sharp change in the solids holdup corresponds to that large increase of pressure drop indicated above in this study as well as those reported by Yerushalmi and Cankurt (1979) and Xu et al. (2001). Therefore, it further substantiates the choking initiation mechanism by means of the collapse of the dense core region or the burst of the blob. With further increase in the solids circulation rate beyond the choking transition, the solids holdups and their fluctuations do not change much. At the lower part of the bed where choking occurs, the time-averaged solids holdups do not undergo further change with increasing solids circulation rate. Rather, the height of the dense bed expands with increasing solids circulation rate until, supposedly, the next dense level is reached. Little is known regarding the state of the bed under the condition with dense bed expansion.

Figure 13a shows the time-averaged radial solids concentration distributions at the lower part of the riser at gas velocities below U_{tr}. At a gas velocity of 0.97 m/s, when the solids circulation rate is 1.32 kg m^{-2} s^{-1}, the solids holdup initially increases to a local maximum value at $r/R = 0.2$, then decreases to the minimum value at $r/R = 0.6$, and finally increases gradually to the maximum value at the wall. This is quite consistent with the double solids-ring flow structure observed by the ECT. The region where r/R is smaller than 0.2 is the dilute gas core region; the region where r/R is between 0.2 and 0.4 is the solids ring at the center region of the bed; the solids ring near the wall is located at r/R larger than 0.8; and the region where $0.4 < r/R < 0.8$ is the gas ring between the two solids rings. The solids holdup in the gas ring is near 0, which is also much lower than that in the dilute core region, indicating that there is a distinct boundary between the core and wall regions. The solids holdup in the solids ring at the center region is comparable to that in the solids ring near the wall of the bed.

The results obtained by the optical-fiber probe show a similar variation of the solids holdup distribution along the radial direction, which further reaffirms the ECT results. However, the solids holdup in the gas ring measured by the optical-fiber probe is higher than that measured by the ECT and the solids holdup in the wall region measured by the optical-fiber probe is lower than that by the ECT. This is, in part, because the optical-fiber probe is not sufficiently sensitive to the measurement of the solids holdup when the bed is very dilute. Also, the probe could interfere with the main flow in the bed yielding effects more remarkable at low solids holdup conditions. Du et al. (2003) gave a detailed comparison between these two techniques of measuring solids concentration in fluidized beds. With an increase in the solids circulation rate to 2.3 kg m^{-2} s^{-1}, the solids holdup is high at the center, then decreases to the minimum value at $r/R = 0.6$, and finally increases to the maximum value at the wall. The region at $r/R < 0.4$ corresponds to the solids core region with a relatively high solids concentration. The other two regions, including the gas ring and the solids ring near the wall, are in the same location as those for $G_s = 1.32$ kg m^{-2} s^{-1}. The solids holdups in the solids core region and in the solids ring near the wall are comparable and both increase with increasing solids circulation rate. The size and the solids holdup in the gas ring do not change much with increasing solids circulation rate before choking. The radial solids concentration profile at a gas velocity of 1.46 m/s and a solids circulation rate of 7.26 kg m^{-2} s^{-1} is also shown in the figure.

The solids concentration profiles for the two operation conditions with the gas velocities below U_{tr} are practically identical before the choking transition. Both of the solids concentrations at the solids core region are about 0.09, which indicates that there could be a critical solids concentration at the solids core region $\epsilon_{s,c}$, making the onset of choking transition for the gas velocities below U_{tr}. When the solids concentration at the solids core region is lower than $\epsilon_{s,c}$, the blobs appear at the center of the bed, whereas the blobs break up and the solids core region collapses when the solids concentration is higher than $\epsilon_{s,c}$. When the solids circulation rate increases to 4.95 kg m^{-2} s^{-1} after choking, the solids holdup increases gradually along the radial direction. The solids holdups at the center of the bed measured by the optical-fiber probe are slightly higher than those measured by ECT and are similar near the wall. Compared to the solids-batch turbulent fluidization system, the radial solids holdup distribution exhibits a similar trend. The only difference is that the solids holdup in turbulent fluidization is higher than that in the circulating system. The radial solids concentration profile shows a similar tendency under the after-choking condition at a gas velocity of 1.46 m/s and a solids circulation rate of 9.91 kg m^{-2} s^{-1}, although the solids holdup is much lower because of the higher gas velocity.

Figure 13b shows the radial solids holdup distributions at the upper part of the riser for both of the two gas velocities below U_{tr}. Under different solids circulation rates, the solids holdup shows a similar trend. The solids holdup remains unchanged at first, increases to the local maximum value, then decreases to the local minimum value, and finally increases to the maximum toward the wall. It corresponds to the double solids-ring flow structure. Compared to the lower part of the riser, the solids ring at the center expands outward to $r/R = 0.5$. At the gas velocity of 0.97 m/s, the solids holdups in the dilute core region and the gas ring are almost the same and they do not change much with increasing solids circulation rate. However, at the gas velocity of 1.46 m/s, the solids holdup in the dilute core region is higher than that in the gas ring, particularly under the operation condition with higher solids circulation rate. For both of the two gas velocities, it is observed that the solids holdup in the gas ring remains almost unchanged with the solids circulation rate. The solids holdups in the two solids rings increase with an increase in the solids circulation rate, especially in the solids ring near the wall.

Dynamic behavior of a CFB at $U_g > U_{tr}$

Figure 14 illustrates the quasi-3D solids holdup distribution at the lower part of the riser under different solids circulation rates at a higher gas velocity of 1.94 m/s. Under all operation conditions examined in this study, a solids core with various solids concentrations at the center, a solids ring near the wall, and a gas ring between these two dense regions are observed across the bed. At a lower solids circulation rate of 6.6 kg m^{-2} s^{-1}, the solids holdup in the solids core region is similar to that in the dense wall region, as shown in Figure 14a. The boundaries between the gas ring and the two dense regions are indistinct, indicating that the exchange of particles between the solids core and solids ring near the wall is extensive. Compared to the lower gas velocity, the area of the solids core region is

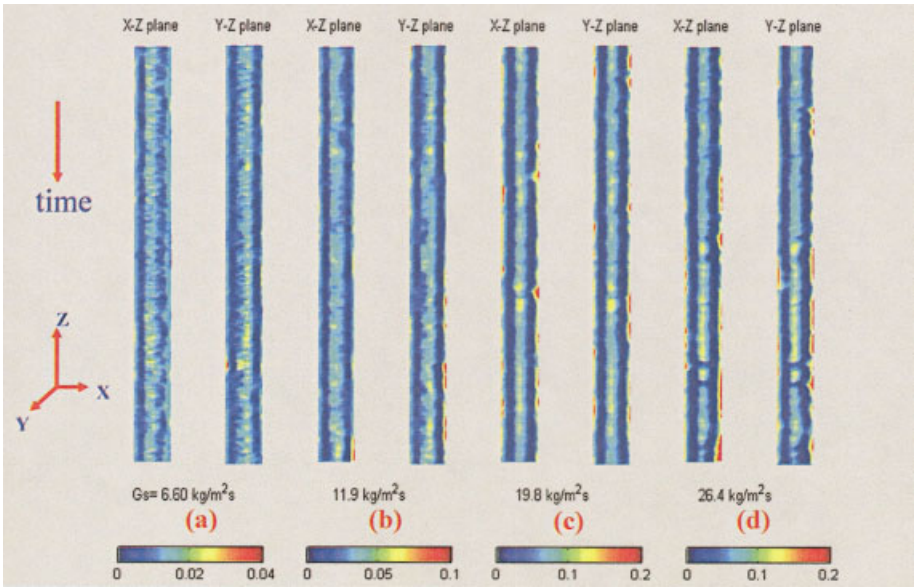

Figure 14. Quasi-3-D flow structures at lower part of a CFB riser at a gas velocity of 1.94 m/s.

almost the same but the dense wall region becomes thinner. With an increase in the solids circulation rate to 11.9 kg m^{-2} s^{-1}, as shown in Figure 14b, the solids holdup increases in both the solids core and the solids ring, especially in the solids ring near the wall. The area of each region does not vary. The boundaries between the gas ring and the two dense regions become relatively clearer, although the particle exchange still occurs frequently.

With further increases in the solids circulation rate to 19.8 kg m^{-2} s^{-1}, the area of the solids core region becomes smaller but the solids holdup increases, as shown in Figure 14c. The blobs with different sizes and shape are formed. The dense wall region becomes thicker and the solids holdup largely increases. The gas ring between the solids core and the solids ring becomes larger and the solids holdup in this region is very dilute, indicating the small amount of particle exchange that occurs in this region. Under this solids circulation rate, a large number of particles or clusters in the dense wall region move downward, whereas the particles or blobs in the solids core region move upward at a high velocity. Under a lower solids circulation rate, the particles or blobs still move upward fast in the center of the bed. However, the particles or clusters in the dense wall region may move either upward or downward at a very low velocity. It is also shown that the blobs in the dense core region tend to connect to each other, forming the blob jets, and move upward continuously in the riser.

With further increase in the solids circulation rate to 26.4 kg m^{-2} s^{-1}, the blob jets are disintegrated into small blobs, as

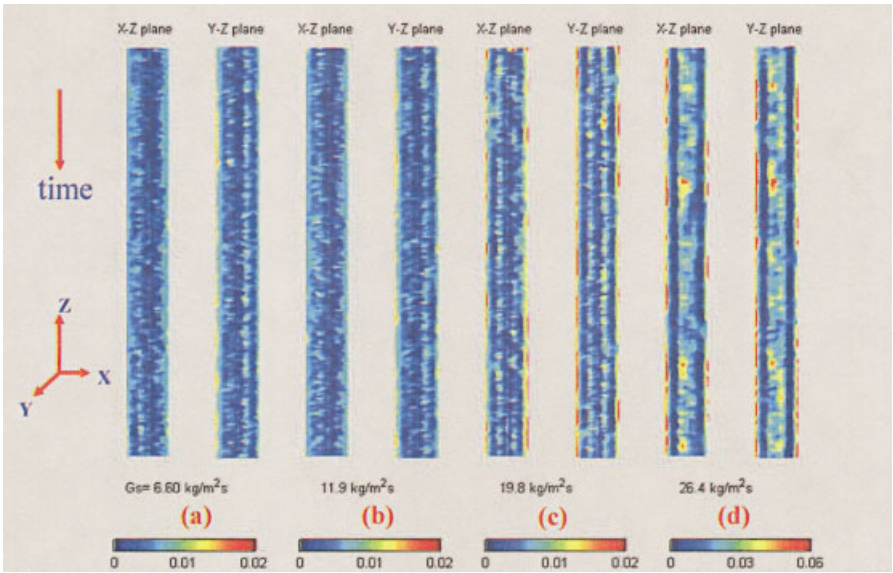

Figure 15. Quasi-3-D flow structures at upper part of a CFB riser at a gas velocity of 1.94 m/s.

shown in Figure 14d. These separated blobs move upward discontinuously in the riser. The solids holdup in the dense wall region increases substantially, especially at the time when the solids holdup in the separated blobs is very low. It is observed that no collapse of solids core region or burst of blobs occurs at the lower part of the riser when the gas velocity is higher than U_{tr}. Correspondingly, there is no sharp change in the pressure drop, which is consistent with that shown in Figure 1. Therefore, the choking transition in the riser under this operation condition is different from that under gas velocities below U_{tr}.

Based on the analysis of the flow structure in the riser, the regime transition can be described. At a lower solids circulation rate, the entire bed tends to be uniform and the boundaries between the three regions are indistinct. The flow system is under the dilute transport regime, corresponding to the region with low pressure drop below dash-dot line in Figure 1a. With an increase in the solids circulation rate, the solids holdup in the solids core region increases to form blobs, indicating the riser transits to the fast fluidization regime. It is known that this regime is characterized by a dense region at the bottom of a riser and a dilute region at the top. The increase in the solids circulation rate contributes mostly to the formation of the blob jets and the increase of the solids holdup in the dense wall region at the bottom of the riser. Therefore, the pressure drop significantly increases, as shown in Figure 1.

With a further increase in the solids circulation rate, the bed is in the dense-phase fluidization regime. However, this regime is different from solids-batch dense-phase fluidization. Because of the high intensity of gas flow, there is no slug formed in the riser. The gas moves upward in the form of bubbles or voids. These small and violent bubbles/voids do not break up the whole blob but render the blob jet separated into small blobs. The pressure drop does not change much in this regime. Similar to the situation at the gas velocities below U_{tr}, this flow structure will be maintained until, supposedly, the next dense level. Therefore, there is no structure variation during the regime transition either from dilute transport to fast fluidization or from fast fluidization to dense-phase fluidization.

Examining the correlations available in the literature, the equations of Yang (1975) and Bi and Fan (1991) could predict well the present data for the regime transition from the dilute transport to fast fluidization regimes. The equations of Bi and Fan (1991) and Xu et al. (2001) could predict well the present data for the regime transition condition from the fast fluidization to the dense-phase fluidization regimes. The prediction of the solids circulation rate by the equation of Yousfi and Gau (1974) for the choking transition to dense-phase fluidization yields a higher value compared to the present data. Takeuchi et al. (1986) noted that the critical gas velocity from fast fluidization to dense-phase fluidization is sensitive to the height of the fluidized bed. Yousfi and Gau (1974) did not consider the effects of bed diameter and height in their equation. Because the variation of the flow structure or the regime transition initiates at the bottom of the riser and then moves upward, the measurement position also affects the outcome of the reported results. A higher measurement position results in a larger solids circulation rate to reach the choking point at a given gas velocity. The results of Yousfi and Gau (1974) are obtained at the fully developed region of the riser, which gives rise to a higher value of the choking transition solids circulation rate compared to that obtained in this study.

Figure 15 shows the solids holdup distribution at the upper part of the riser under different solids circulation rates at a higher gas velocity of 1.94 m/s. Based on the analysis of the regime transition given above, Figure 15a and b show the flow structure at low solids circulation rates of 6.6 and 11.9 kg m^{-2} s^{-1}, respectively, in the dilute transport regime. The flow structures are very similar in these two conditions. Both of them exhibit the double solids-ring structure with intense solids exchange between the two solids rings. With further increase of solids circulation rate to the fast fluidization regime, as shown in Figure 15c, the double solids-ring structure is clearly seen, although the solids still exchange frequently between the two solids rings. The solids holdup in the solids ring near the wall increases appreciably. Figure 15d shows the flow structure in the dense-phase fluidization regime. The solids core is observed. The solids holdups in both the solids core region and the dense wall region increase significantly. The boundaries between the gas ring and these two dense regions become much clearer, reflecting less solids exchange between the upward flowing blob in the solids core region and the downward flowing particles/clusters in the dense wall region. Therefore, in the upper part of the riser, there are no clear boundaries between different flow regimes based on the measured flow structure.

Figure 16 shows the 20-s time averaged cross-sectional solids holdup distribution at different solids circulation rate in planes 1 and 2 at both the lower part and upper part of the riser. Three sets of images represent the three fluidization regimes—that is, dilute transport, fast fluidization, and dense fluidization regimes—from lower to higher solids circulation rate. The overall solids holdup increases with increasing solids circulation rate. Similar to the lower gas velocity ($<U_{tr}$), the time-averaged cross-sectional solids holdup at a higher gas velocity also exhibits a radial symmetric distribution under all solids circulation rates, especially at higher solids circulation rates. At the lower part of the riser, with an increase in the solids circulation rate, the solids core region shrinks gradually, whereas the dense wall region becomes thicker and its solids holdup becomes higher. Regarding the two planes in the figure, the solids holdup at a lower level (plane 1) is higher than that at a higher level (plane 2). The solids holdups in the solids core region and in the wall region all reduce from plane 1 to plane 2 in the dilute transport regime. However, in the fast fluidization and the dense fluidization regimes, the solids core region becomes denser but the dense wall region becomes more dilute from plane 1 to plane 2. Because the flow tends to be uniform in the dilute transport regime, more particles are carried into the solids core region from the dense wall region, especially at the bottom of the riser. Therefore, the solids core region is large and the solids holdup in the dense core region in plane 1 is higher than that in plane 2. Moreover, the particles are transported intensively between these two dense regions.

In the fast fluidization regime, the flow is nonuniform. The particles form blobs or blob jets in the solids core region, which explains the shrinkage of the solids core region; but the solids holdup increases with increasing solids circulation rate. Simultaneously, the blobs or blob jets might be disintegrated because of the violent upward flowing gas. The gas at the bottom of the riser has the highest internal energy. The blob jets are disinte-

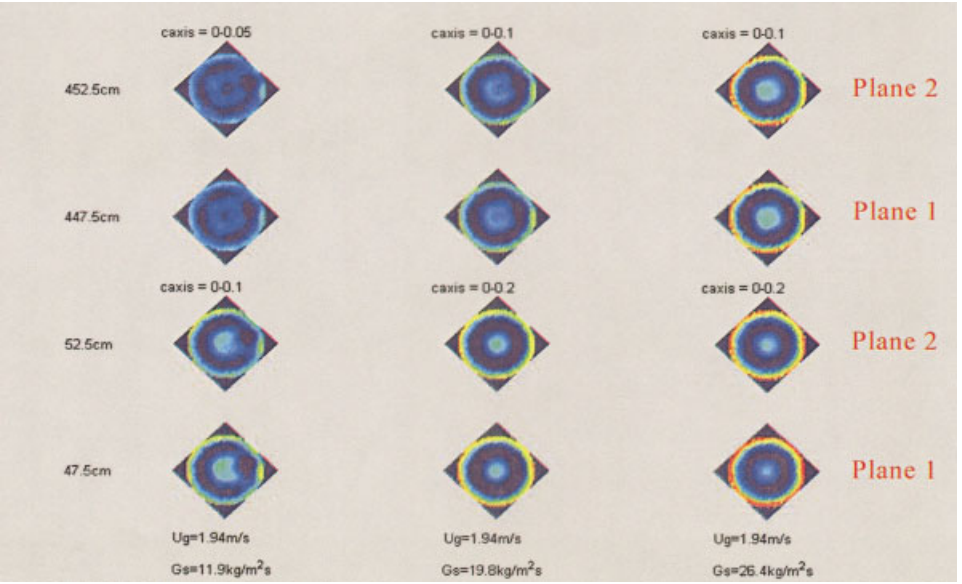

Figure 16. Time-averaged cross-sectional solids holdup distributions at a gas velocity of 1.94 m/s.

grated easily and some particles are ejected to the dense wall region. Therefore, the solids holdup in the solids core region in plane 1 is lower than that in plane 2, whereas the dense wall region in plane 1 is denser than that in plane 2. In the dense fluidization regime at high solids circulation rate, the flow structure is similar to that in the fast fluidization regime.

The presence of a lower solids holdup in the solids core region and a much higher solids holdup in the dense wall region is remarkable. It can be attributed to the fact that the blobs are broken up by the violent bubbles and more particles are ejected to the dense wall region, especially at the lower level of the riser. At the upper part of the riser, the solids holdups are comparable to those at the lower part of the riser. The flow structure in the dilute transport and the fast fluidization regimes is the double solids-ring structure, whereas in the dense fluidization regime the solids core region is formed. The solids holdup in both the center of the bed and the wall region increases with increasing solids circulation rate. The area, occupied by the gas core and the solids ring at the center for the double solids-ring structure or occupied by the solids core, reduces gradually from the dilute transport, the fast fluidization to the dense fluidization regimes. However, the area of the solids ring near the wall or the dense wall region remains almost unchanged. At the dilute transport regime, the solids ring at the center region of the bed tends to expand toward the wall to render uniform gas–solids flow, reflected by its asymmetric solids holdup distribution and the indistinct boundary between the two rings. With increasing solids circulation rate in the fast fluidization regime, particles tends to bundle with each other, which increases the solids holdup in both the solids ring at the center and the gas core and reduces the occupied area. Finally, the blobs or blob jets appear with further increase in the solids circulation rate in the dense-phase fluidization regime, which in turn reduces the occupied area and increases the solids holdup.

The transient cross-sectional solids holdup distributions measured by ECT at the lower part of the riser under different solids circulation rates are shown in Figure 17. In the dilute transport regime at a lower solids circulation rate as shown in lines (a) and (b), both the solids holdups and their fluctuations are very small, reflecting the uniform flow and slight backmixing in the bed. With the increase of the solids circulation rate to the fast fluidization regime, both the solids holdups and their fluctuations substantially increase, as shown in line (c), which indicates a heterogeneous flow structure in this flow regime with upward flowing blobs in the center of the bed and downward flowing particles/clusters in the wall region. Line (d) shows the solids holdup profile in the dense-phase fluidization regime. Both the solids holdups and their fluctuations further increase, indicating the turbulent flow behavior in this regime. It is also seen that the solids holdup is lower during the time period from 1 to 5 s but much higher in other time periods, which can be attributed to the violent movement of bubbles and particles in the bed. The particles at the lower part of the riser are carried quickly upward to some extent by the bubbles forming a relatively low solids holdup region. The bed is then collapsed and the particles aggregate at the bottom of the bed,

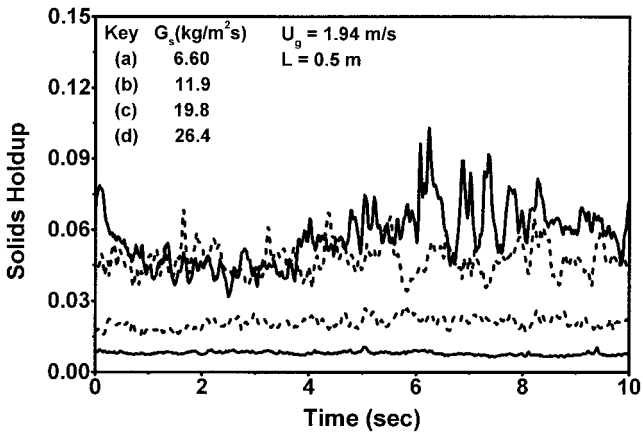

Figure 17. Transient solids holdup distributions at lower part of a riser at a gas velocity of 1.94 m/s.

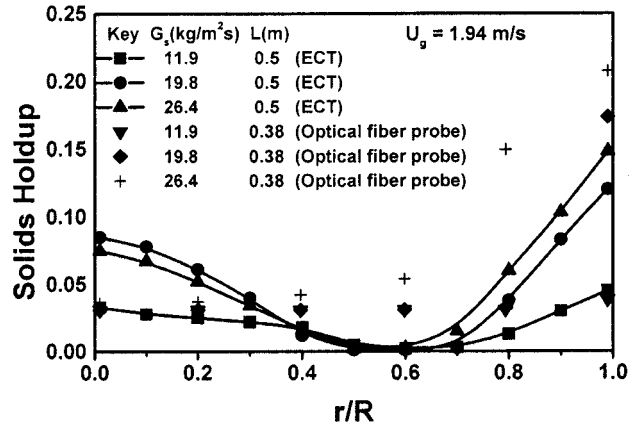

(a) Lower part of a riser

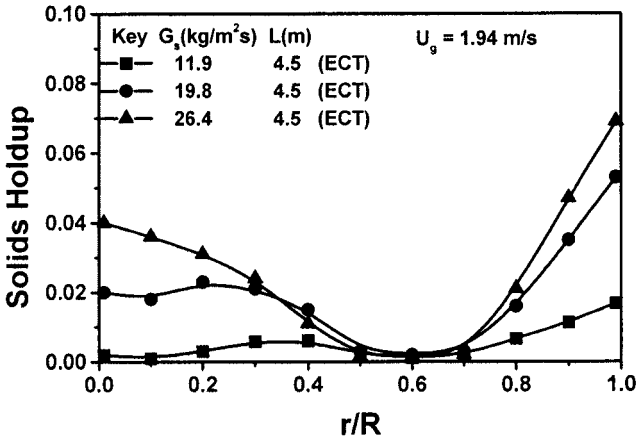

(b) Upper part of a riser

Figure 18. Radial solids holdup distributions at a gas velocity of 1.94 m/s.

forming the relatively high solids holdup region over a period of time. Compared to the situation at a lower gas velocity, there is no sharp change of solids holdup and no structure variation during the regime transition. The solids holdup increases slightly in the dilute transport regime and in the dense-phase fluidization regime, whereas it increases substantially in the fast fluidization regime. This is consistent with the variation of pressure drop with the solids circulation rate at the gas velocity of 1.94 m/s, as shown in Figure 1.

Figure 18a shows the time-averaged radial solids concentration distribution at the lower part of the riser at the gas velocity of 1.94 m/s. Under all operation conditions, the solids holdup is high at the center, then decreases to the minimum value at $r/R = 0.6$, and finally increases to the maximum value at the wall. The region at $r/R < 0.4$ corresponds to the solids core region with a relatively high solids concentration. The solids core near the wall is located at $r/R > 0.8$. The gas ring is located between the solids core and the solids ring. The solids holdups in the solids core region and in the solids ring near the wall are comparable. The solids holdup in the solids ring near the wall increases with increasing solids circulation rate. However, as the solids circulation rate increases, the solids holdup in the solids core increases from dilute transport to fast fluidization regimes but decreases from fast fluidization to dense-phase fluidization regimes. Similar to the situation in the lower part of riser at gas velocities below U_{tr}, the solids holdup in the gas ring is nearly 0. The size and the solids holdup in the gas ring do not change much with increasing solids circulation rate.

The results measured by the optical-fiber probe are also shown in the figure. In the dilute transport regime, the radial solids holdup distribution is very flat. With the increase of the solids circulation rate to the fast fluidization regime, the solids holdup in the core region does not change much, whereas the solids holdup in the wall region substantially increases. In the dense-phase fluidization regime, the solids holdup increases gradually along the radial direction. These results from the optical-fiber probe are consistent with those in the literature and the typical core–annular model for the fast fluidization regime. The cross-sectional averaged solids holdups measured by the optical-fiber probe may be the same as those measured by the pressure transducer and the ECT. However, the optical-fiber probe measurement is not sensitive to the low solids holdup condition. For low solids holdups, it cannot accurately measure the solids holdup along the radial direction to allow flow structure to be identified in a CFB riser. Compared to the solids-batch turbulent fluidization system, the radial solids holdup distribution in the dense-phase fluidization regime is different when the gas velocity is greater than U_{tr}. Therefore, for a solids circulating system, the dense-phase fluidization regime can be divided into two types based on the gas velocity relative to U_{tr}, as shown in Figure 6.

Type I is for the gas velocities below U_{tr} where the flow structure is similar to the solids-batch dense-phase fluidization. Type II is for the gas velocities above U_{tr} where the flow structure is different from the solids-batch dense-phase fluidization. Figure 18b shows the radial solids holdup distributions at upper part of the riser. In the dilute transport regime, the bed exhibits the double solids-ring flow structure. The solids ring at the center region is located at $0.1 < r/R < 0.5$. Along the redial direction, the solids holdup does not change much, reflecting a relatively homogeneous flow behavior in this regime. With an increase in the solids circulation rate to the fast fluidization regime, the solids ring at the center region shrinks to $0.1 < r/R < 0.4$. In the dense-phase fluidization regime, the solids core region is formed and the solids holdup decreases to a minimum value first and then increases toward the wall along the radial direction. The solids holdups in the solids core region and in the wall region all increase with increasing solids circulation rate, whereas the solids holdup in the gas ring between the core and wall regions remains unchanged at a low solids concentration. Under all solids circulation rates, the solids holdup in the core region is comparable to that in the wall region.

Effects of solids feeding pattern and relative humidity on the flow structure of a CFB

The results presented thus far are based on the solids feeding to the bottom of the riser through the L-valve as shown in Figure 19a. To examine the solids feeding and solids distribu-

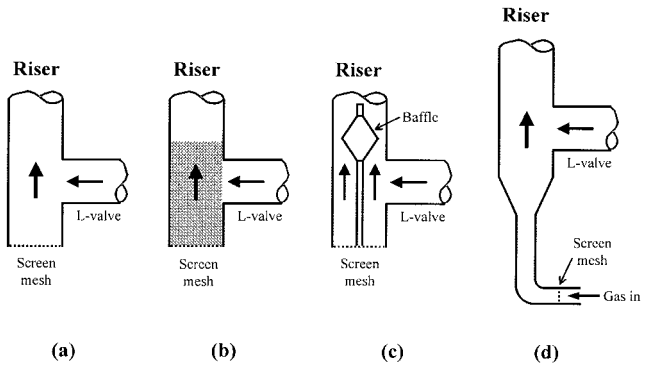

Figure 19. Diagram of the solids feeding patterns.

tion effects on the flow structure and hence the choking phenomenon of the riser, three other types of solids feeding patterns are considered and their results are compared with those from the L-valve feeding pattern. The details of these three solids feeding patterns are given in Figure 19b–d. For solids feeding pattern (b), large cylindrical particles are filled in a packed bed at the bottom of the riser. Solid particles from the downcomer enter the riser from the side of the packed bed and thus are well dispersed across the bed. For solids feeding pattern (c), an internal is placed at the bottom of the riser such that the gas and the solids are dispersed outward as they enter the riser. For solids feeding pattern (d), gas enters the riser through a tapered section with the solids retaining mesh placed far upstream.

Figure 20 shows the effects of solids feeding patterns on the flow structure in a CFB riser under a gas velocity of 0.97 m/s and a solids circulation rate of 0.99 kg m^{-2} s^{-1}. The four groups of images correspond to the four solids feeding patterns as shown in Figure 19. There are two solids rings near the wall and around the gas core respectively and a gas ring between these solids rings in Figure 20a, especially in the Y–Z plane. It is similar to that in Figure 8a with a higher solids circulation rate. The boundaries between these regions across the bed are indistinct, indicating the severe radial particles interchange. When the solid particles are well dispersed before moving upward in the bed for solids feeding pattern (b), although the solids holdup in this condition is lower than that for solids feeding pattern (a), the whole bed exhibits three regions across the bed with a solids ring near the wall, a solids core at the center, and a gas ring between them. Solids feeding pattern (c) does not break up the typical double solids-ring flow structure. However, because of the presence of the internal, particles are forced to move outward. Thus, the gas core at the center of the bed is enlarged and the area occupied by the gas ring between the two solids rings is reduced. For solids feeding patterns (d), the flow structure does not change much compared to that for solids feeding pattern (a), with the exception of the extent of the solids concentration in each region across the bed.

The ECT studies indicate that as the solids circulation rate increases before the choking transition, the bed for all the four solids feeding patterns exhibits the ring structure with a solids ring near the wall, a gas ring adjacent to it, and a solids core at the center. It is noted that the extent of the solids concentration in the structure varies with the feeding patterns. Beyond the choking transition, the flow structure for a CFB is similar to that for a solids-batch dense-phase fluidized bed. The solids circulation rate at the point of the choking transition is different for each solids feeding pattern. At a low gas velocity ($<U_{tr}$), the solids feeding pattern affects the flow structure only under the low solids circulation rate condition. When the solids circulation rate is high, the solids feeding pattern has no effect on the flow structure and the choking transition. This behavior can be attributed to the fact that the flow structure is influenced not only by the solids feeding pattern but also by the solids recirculation in the bed. Under dense operation conditions, a

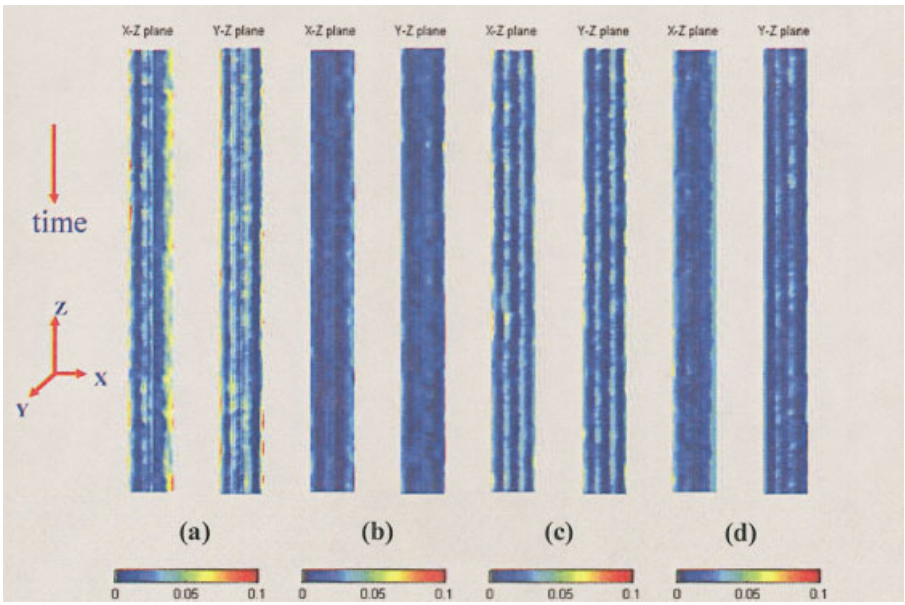

Figure 20. Effect of solids feeding patterns on the flow structure of a CFB riser at U_g = 0.97 m/s and G_s = 0.99 kg m^{-2} s^{-1}.

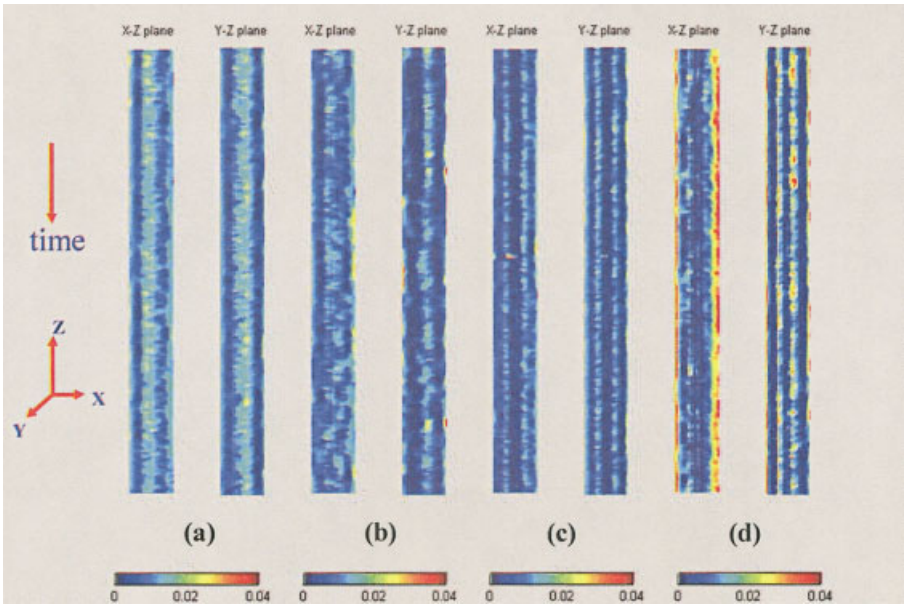

Figure 21. Effect of solids feeding patterns on the flow structure of a CFB riser at U_g = 1.94 m/s and G_s = 6.6 kg m^{-2} s^{-1}.

large number of particles or clusters moving downward along the wall exchange between the core region and the wall region, which contributes to maintain the typical flow structure and choking transition in a CFB riser.

The effects of solids feeding patterns on the flow structure at a higher gas velocity of 1.94 m/s and a solids circulation rate of 6.6 kg m^{-2} s^{-1} are shown in Figure 21. The flow structure for solids feeding pattern (b) is similar to that for solids feeding pattern (a) with the three regions across the bed. However, because the particles are well dispersed before moving upward, the boundaries between the different regions across the bed are indistinct and the radial solids concentration distribution is uniform, as shown in X–Z plane in Figure 21b. The effect of the internal for solids feeding pattern (c) on the flow structure is remarkable. The particles are forced to move outward, forming a large gas core in the bed. The two solids rings around the gas core and near the wall are almost integrated through the gas ring between them, as shown in Figure 21c. When the gas distributor is removed, the entire bed exhibits a double solids-ring flow structure, as shown in Figure 21d, particularly in Y–Z plane. With further increases in the solids circulation rate to the fast fluidization regime or the dense-phase fluidization regime (II), the flow structures for different solids feeding patterns remain unchanged except that the solids concentration in each region across the bed increases, particularly near the wall region. Therefore, at the higher gas velocity ($>U_{tr}$), solids feeding patterns (c) and (d) move the particles away from the central core region to form a solids ring around a gas core. It is noted that the ring structure is retained under the four diverse solids feeding patterns and the solids recirculation from the wall region and the solids exchange between the core region and the wall region contribute significantly to the formation of this inherent structure in a CFB riser.

In a CFB riser, particle electrification can occur through the collisions of particle–wall and particle–particle. The electrostatic force plays a significant role in determining the heterogeneous flow structure of gas–solid pneumatic systems (Al-Adel et al., 2002). Jiang et al. (1996) studied the electrostatic charge effects, using the same experimental apparatus as this study, on the local solids distribution in the upper region of circulating fluidized beds. From the optical-fiber probe and the Faraday cage measurements, they found that for FCC particles, the solids concentration in the core region increases with the relative humidity, whereas in the wall region it exhibits an opposite trend, which is attributed to the reduced attraction forces between particles and the wall caused by the electrostatic forces. Their study also indicated that the variation of the solids concentration or holdup with the relative humidity can be negligible when the relative humidity is larger than 20% over the gas and solids circulation rate considered in this study. This study examines the effect of the relative humidity of 6.5, 20, and 40%. All the experimental results reported here, unless otherwise noted, are obtained at a gas relative humidity of 6.5%. Figure 22 shows the flow structure under the relative humidity of 6.5, 20, and 40% at the lower part of a CFB riser. At a lower gas velocity of 0.97 m/s, the basic flow structures at different relative humilities are comparable with the existence of the solids core region at the center of the bed, as shown in Figure 22a at a solids circulation rate of 2.3 kg m^{-2} s^{-1}. The area occupied by the solids core region decreases as the gas humidity increases from 6.5 to 20% but increases as the gas humidity varies from 20 to 40%.

The electrostatic forces of particle–particle and particle–wall decrease with increasing relative humidity. Therefore, as the relative humidity increases from 6.5 to 20%, the aggregation tendency for the particles to form the blobs at the center and clusters at the wall region of the bed is weakened correspondingly. More particles tend to move as particle groups and are easily carried upward to the upper region of the bed. The solids holdup difference between the lower part and upper part is

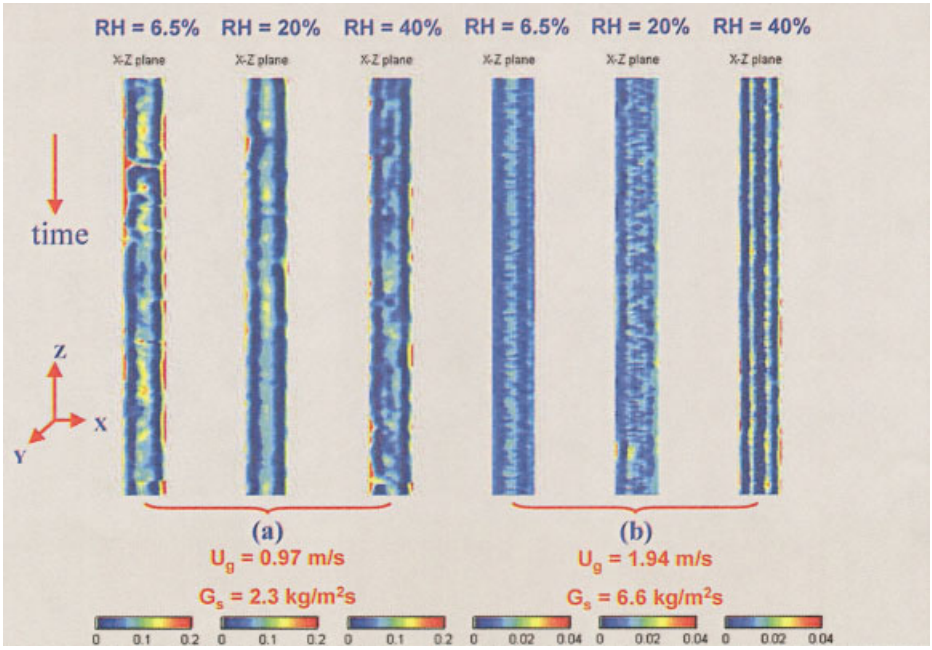

Figure 22. Effect of relative humidity on the flow structure of a CFB riser.

reduced and the entire bed in the axial direction is more uniform under a higher relative humidity condition. With an increase in the gas humidity to 40%, the electrostatic forces of particle–particle and particle–wall further decrease, rendering reduced formation of particle groups and enhanced exchange of solids in the radial direction, leading to enlarged solids core region. The cross-sectional averaged solids holdups are comparable at 0.073, 0.069, and 0.076 for the relative humidities of 6.5, 20, and 40%, respectively. From the experimental results, under a high relative humidity, the bed undergoes a similar regime transition with increasing solids circulation rate at a given gas velocity to that under a low relative humidity. The choking still occurs when the blobs disintegrate and the bed suspension collapses, although the solids circulation rate at the choking transition at a given gas velocity increases under a high relative humidity condition.

At a higher gas velocity of 1.94 m/s, when the gas humidity increases from 6.5 to 20%, the solids exchange between the two dense regions becomes intense as a consequence of the low electrostatic forces and the bed also exhibits a uniform distribution in both the axial and the radial direction, as shown in Figure 22 (b) at a solids circulation rate of 6.6 kg m^{-2} s^{-1}. However, when the gas humidity increases from 20 to 40%, it is seen that solids in the bed redistribute along the radial direction and the bed exhibits the double solids-ring flow structure. Although there appears to be a variation in flow structure, the cross-sectional averaged solids holdups do not vary appreciably (that is, 0.0080, 0.0066, and 0.0070 for the relative humidities of 6.5, 20, and 40%, respectively). From the experimental results on the flow structure, the bed still undergoes similar regime transitions from the dilute transport regime to the fast fluidization regime to the dense-phase fluidization regime (II), but the transition solids circulation rate at a given gas velocity is different under different relative humidities.

Observations on flow structure variation during choking transition

Based on the results given above, a mechanism on choking initiation and fluidization regime transition can be phenomenologically described. Figure 23 depicts the variation of flow structure at the bottom of the riser with increasing solids circulation rate under a given gas velocity below U_{tr}. Solids at the bottom of the riser, fed from the L-valve and transported downward from the wall region, are carried upward by the gas flow. Because of the low solids circulation rate, gas flows fast at the center of the bed and is surrounded by the upward flowing particles, forming the double solids-ring flow structure. Along the radial positions, particles in the two solids rings are exchanged intensively. Jiang and Fan (1999) examined both the inward and the outward particle transfer rates in the radial direction in a CFB riser using a particle-sampling probe. At a given position in the bed, the radial solids flux in the inward

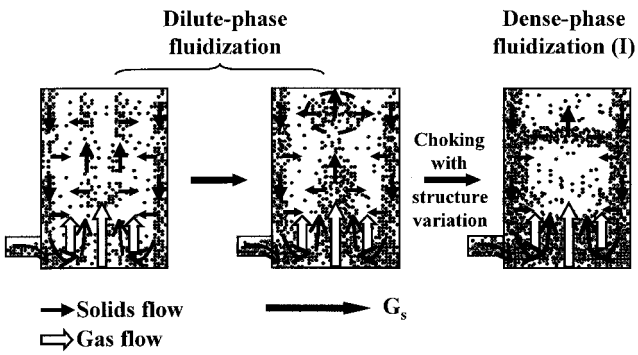

Figure 23. Mechanism of choking and regime transition in circulating fluidized beds at $U_g < U_{tr}$.

direction is almost the same as that in the outward direction. The radial solids flux reaches a maximum value at the transition region between the wall and the core, corresponding to the region between the gas ring and the solids ring near the wall. With the increase of gas velocity, more particles are carried upward at the center of the bed. The solids ring at the center region of the bed expands slightly toward the wall and the area occupied by the dilute core and the solids ring at the center region of the bed is correspondingly enlarged.

Furthermore, the solids exchange between the two solids rings becomes stronger. The boundaries between the different regions across the bed are indistinct. With increasing solids circulation rate in the dilute-phase fluidization regime, the solids holdups in each region across the bed increase significantly. Solids then tend to aggregate to form the blobs or blob jets at the center of the bed or clusters in the wall region. The overall flow structure is transformed from the double solids-ring structure to the three-region structure. The blobs or blob jets and clusters are in the dynamic variation between formation and breakage though the formation process is dominant in this fluidization regime. Similarly, solids exchange occurs frequently between the upward flowing blob or blob jets and the downward flowing clusters. Compared to the clusters in the wall region, the solids holdup in the blobs is lower, reflecting a looser structure between particles in the blobs because of high turbulence of the gas phase in the center of the bed. Increasing gas velocity results in smaller blobs with lower solids holdups. With further increase in the solids circulation rate in the dense-phase fluidization regime, the solids holdup increases continuously in each region across the bed. The solids holdup in the blobs substantially increases. At the same time, more particles are carried into the wake behind the blob or blob jet. It could be that at a time when the upward drag force induced by the gas cannot support the whole movement of the blobs or blob jets, the blobs or blob jets are broken up and the bed suspension at the center of the bed collapses, which marks the choking transition with structure variation. The large gas core region is formed in the bed simultaneously. Because of the violent gas movement, the particles are carried upward quickly and transported to the wall frequently, resulting in the local circulation of particles in the bed. The flow behavior in this regime is similar to the conventional dense fluidization, even though some solids are circulating in the entire system. This is noted as Type I dense-phase fluidization regime, as given in Figure 6. For the upper part of the riser, the bed always exhibits the double solids-ring flow structure. With increasing solids circulation rate at a given gas velocity, the solids holdup in the ring region of the flow structure increases. It is not possible to identify the fluidization regime transition or the choking transition based on the variation of the flow structure at the upper part of the riser.

The flow structure observed by the ECT is different when the gas velocity is greater than U_{tr}. Consequently, the manner in which choking and fluidization regime transition is defined would be different. Figure 24 illustrates the variation of the flow structure at the bottom of a riser with the increase of solids circulation rate at a given gas velocity above U_{tr}. At a lower solids circulation rate in the dilute transport regime, solids at the bottom of the riser are carried upward by the gas, forming a solids core in the bed. Compared to the low gas velocity situation, this solids core is larger in the dilute transport regime.

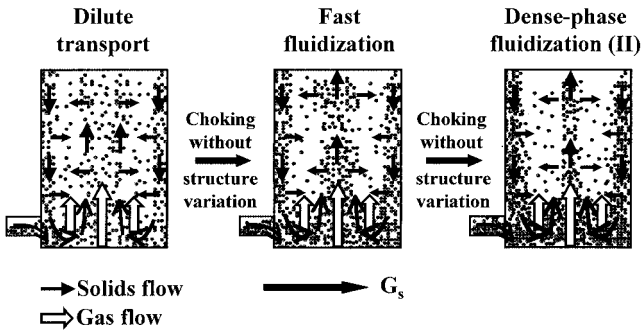

Figure 24. Mechanism of choking and regime transition in circulating fluidized beds at $U_g > U_{tr}$.

In the solids core, the particles move upward. The solids holdup in the solids ring near the wall is slightly higher than that in the solids core. Particles in the solids ring near the wall move downward. The solids exchange in the gas ring between the solids core and the solids ring is intense, reflecting the relative homogeneous flow behavior in this regime. With an increasing solids circulation rate to the fast fluidization regime, there is no variation in the flow structure and the cross section of the bed still exhibits the three regions, including a solids core at the center, a solids ring near the wall, and a gas ring in between. Because of the increase of the solids holdup in each region, particles tend to aggregate in this regime. Therefore, the upward flowing blobs or blob jets are formed in the solids core and the downward flowing clusters are in the solids ring near the wall. Similar to the situation in the lower gas velocity ($<U_{tr}$), the blobs or blob jets and the clusters are in the dynamic behavior between aggregation and disintegration.

Solids also exchange frequently between the solids core and the solids ring near the wall. This regime transition is termed choking transition from dilute transport to fast fluidization regime without structure variation. With a further increase in the solids circulation rate to the dense-phase fluidization regime, the solids core shrinks and the solids concentration in it also decreases, whereas the solids concentration in the solids ring near the wall increases significantly. With the high velocity of the gas, the blobs or blob jets are still suspended at the central region of the bed. However, the gas phase consisting of small bubbles or voids instead of slugs or large bubbles is formed in the bed. The blobs or blob jets are then separated into small aggregates and move outward to the wall region resulting in a low solids concentration in the solids core region. Although it is called dense-phase fluidization, the flow behavior is somewhat different from the solids-batch dense-phase fluidization. Here it is noted as Type II dense-phase fluidization regime, given in Figure 6. The regime transition is noted as a choking transition from the fast fluidization regime to the dense-phase fluidization (II) regime. Therefore, for high gas velocity conditions, the fluidization regime transits gradually and there are no distinct boundaries between them. For the upper part of the riser, the flow structure is similar to that in the lower gas velocity ($<U_{tr}$). The bed exhibits the double solids-ring flow structure and the solids holdup in each region increases with the solids circulation rate at a given gas velocity. When the solids concentration is significantly high, the gas core and the solids ring at the center of the bed could combine to form the solids core region.

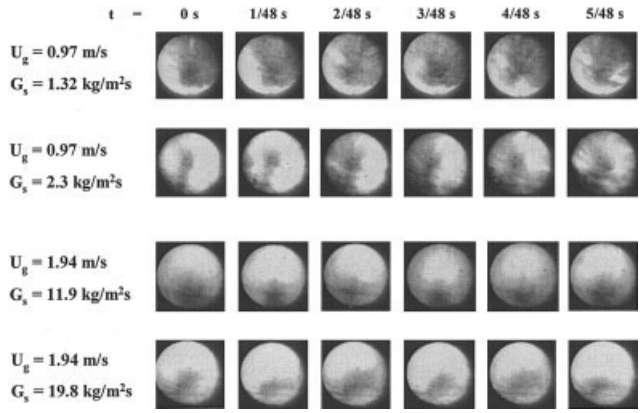

Figure 25. Blob behavior at the center of a CFB riser.

Blob behavior in a CFB riser

To examine the dynamic behavior of the blob further, flow visualization is conducted using the borescope together with the high-speed video camera. Figure 25 shows the blob behavior at the center of the CFB riser at different operation conditions. Six pictures with a time interval of 1/48 s are presented for each solids circulation rate. The diameter of the circular viewing area is 1.5 cm. The degree of brightness reflects qualitatively the extent of the solids concentration in the measurement domain. For the gas velocity of 0.97 m/s, below U_{tr}, at a lower solids circulation rate of 1.32 kg m^{-2} s^{-1}, the bright area is small indicating the low solids holdup in the region. Under this operating condition, solids tend to be less aggregate. With an increase in the solids circulation rate to 2.3 kg m^{-2} s^{-1}, a large bright area with an averaged diameter of 1.0 cm appears, indicating the formation of large aggregates. For the gas velocity of 1.94 m/s, above U_{tr}, the blob size clearly further increases. The solids concentration in the blob increases with increasing solids circulation rate. The averaged diameter of the blob increases from 0.9 to 1.2 cm as the solids circulation rate increases from 11.9 to 19.8 kg m^{-2} s^{-1}, which is consistent with the flow structure obtained by the ECT. The shape and the size of the blob continue to change with the time. Furthermore, the blob may disappear transitorily. All this behavior reflects the dynamic nature of the blob which aggregates and disintegrates periodically.

Based on the analysis of flow structure measured by the ECT, the upward blob velocity can be obtained by the tomography image velocimetry (TIV). The variation of blob velocity with the solids circulation rate at different gas velocities, and lower and upper parts of the bed is shown in Figure 26. The blob velocities under all operating conditions are in the range of 0.5–0.8 m/s. This range of blob velocity is consistent with the calculation based on the mass balance of solid particles across the bed considering the downward cluster flow near the wall as follows:

$$\rho_p U_{blob} A_1(1-\varepsilon_1) + \rho_p U_{cluster} A_2(1-\varepsilon_2) = G_s A \qquad (4)$$

The cluster velocities, $U_{cluster}$ (> -0.3 m/s), obtained by the correlation of Wei et al. (1998) from the laser Doppler velocimetry (LDV) measurement, are used in the calculation. At the upper part of the riser, the blob velocity for the gas velocities of 0.97 and 1.46 m/s increases with an increasing solids circulation rate, whereas it increases initially and then levels off for the gas velocity of 1.94 m/s. At the lower part of the riser, for the gas velocities of 0.97 and 1.46 m/s, blobs do not form after the choking transition in the dense-phase fluidization regime (I) and thus, no blob velocity is reported. The blob velocity at $U_g = 0.97$ m/s is much higher than that at $U_g = 1.46$ m/s. For each gas velocity lower than U_{tr}, the blob velocity does not change much with the solids circulation rate. However, at a higher gas velocity of 1.94 m/s, the blob velocity increases initially in the dilute transport regime, then decreases and levels off in the fast fluidization and dense fluidization regimes. This peak can be noted as the transition between the dilute transport and the fast fluidization regimes. The solids circulation rate for this transition is in agreement with the result obtained by Bi and Fan (1991).

Concluding Remarks

The ECT with NN-MOIRT reveals a double solids-ring flow structure at low solids circulation rates and the formation of a solids core region at high solids circulation rates in a CFB riser with FCC catalyst particles. The flow structure undergoes a distinctive variation with the collapse of the solids core region and the burst of solids blobs during the choking transition when the gas velocity is below U_{tr}. In contrast, when the gas velocity is above U_{tr}, the variations of the solids holdup during the commonly noted choking transitions are not achieved by a distinctive variation of flow structure. The flow structure variations are not appreciably affected by the solids feeding patterns and gas relative humidity.

For the low gas velocities ($<U_{tr}$), the solids holdup in the particle blob measured by the ECT and the blob size observed by the borescope at the center of the bed all increase as the solids circulation rate increases. The disintegration of the enlarged blobs or blob jets and the collapse of the solids suspension characterize the mechanics of the initiation of the choking transition to the dense-phase fluidization regime attributed to solids suspension instability. The ECT results obtained in this study provide new insight into the formation and the instability

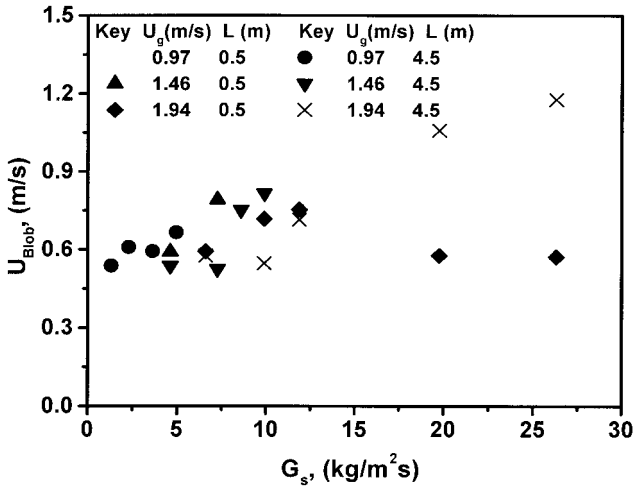

Figure 26. Variation of upward flowing blob velocity with the solids circulation rate.

of the flow structure on which efforts on the computational fluid dynamics should be placed.

Acknowledgment

This article was presented as Paper No. 140c at the AIChE Annual Meeting, Indianapolis, IN, Nov. 2002.

Notation

A = cross-sectional area of the bed, m^2
A_1 = cross-sectional area occupied by the blobs, m^2
A_2 = cross-sectional area occupied by the clusters, m^2
Ar = Archimedes number
D_t = bed diameter, m
G_s = solids circulation rate, kg m^{-2} s^{-1}
$G_{s,tr}$ = transport solids circulation rate, kg m^{-2} s^{-1}
$\Delta P/\Delta Z$ = pressure drop gradient, kPa/m
r = radial position in the bed, m
R = radii of the bed, m
Re_t = particle Reynolds number, based on particle diameter and particle terminal velocity
U_{blob} = upward flowing velocity of blob, m/s
$U_{cluster}$ = velocity of the clusters, m/s
U_{fd} = upper bound of the gas velocity for the fast fluidization regime, m/s
U_g = superficial gas velocity, m/s
U_p = superficial solids velocity, m/s
U_{tr} = transport velocity, m/s
U_{tf} = lower bound of the gas velocity for the fast fluidization regime, m/s

Greek letters

ϵ = overall voidage of the bed
$\epsilon_{s,c}$ = critical solids concentration at the solids core region.
ϵ_1 = voidage of the region occupied by the blobs
ϵ_2 = voidage of the region occupied by the clusters
γ = parameter defined in Eq. 1
ρ_g = gas density, kg/m^3
ρ_p = particle density, kg/m^3

Literature Cited

Al-Adel, M. F., D. A. Saville, and S. Sundaresan, "The Effect of Static Electrification on Gas–Solids Flows in Vertical Risers," *Ind. Eng. Chem. Res.*, **41**, 6224 (2002).

Beck, M. S., and R. A. Williams, "Process Tomography: A European Innovation and Its Application," *Meas. Sci. Technol.*, **7**, 215 (1996).

Bi, H. T., and L.-S. Fan, "Regime Transition in Gas–Solid Circulating Fluidized Beds," *AIChE Annual Meeting*, Los Angeles, CA, Nov. 17 (1991).

Bi, H. T., and J. R. Grace, "Flow Regime Diagrams for Gas–Solid Fluidization and Upward Transport," *Int. J. Multiphase Flow*, **21**(6), 1229 (1995).

Bi, H. T., J. R. Grace, and J. X. Zhu, "Types of Choking in Vertical Pneumatic Systems," *Int. J. Multiphase Flow*, **19**(6), 1077, 1993.

Capes, C. E., and K. Nakamura, "Vertical Pneumatic Conveying: An Experimental Study with Particles in the Intermediate and Turbulent Flow Regimes," *Can. J. Chem. Eng.*, **51**, 31 (1973).

Day, J. Y., H. Littman, and M. H. Morgan III, "A New Choking Velocity Correlation for Vertical Pneumatic Conveying," *Chem. Eng. Sci.*, **45**(1), 355 (1990).

Du, B., L.-S. Fan, F. Wei, and W. Warsito, "Gas and Solids Mixing in a Turbulent Fluidized Bed," *AIChE J.*, **48**(9), 1896 (2002).

Du, B., W. Warsito, and L.-S. Fan, "Bed Non-homogeneity in Turbulent Gas–Solid Fluidization," *AIChE J.*, **49**(5), 1109 (2003).

Dyakowski, T., R. B. Edwards, C. G. Xie, and R. A. Williams, "Application of Capacitance Tomography to Gas–Solid Flows," *Chem. Eng. Sci.*, **52**, 2099 (1997).

Dyakowski, T., L. Jeanmeure, and A. Jaworski, "Applications of Electrical Tomography for Gas–Solids and Liquid–Solids Flows—A Review," *Powder Technol.*, **112**, 174 (2000).

George, D. L., J. R. Torczynski, K. A. Shollenberger, T. J. O'Hern, and S. L. Ceccio, *Quantitative Tomographic Measurements of Opaque Multiphase Flows*, Sandia Report SAND2000-0441, Sandia National Laboratories, Livermore, CA (2000).

Jiang, P., and L.-S. Fan, "On the Turbulent Radial Transfer of Particles in a CFB Riser," *Circulating Fluidized Bed Technology VI*, J. Werther, ed., DECHEMA, Frankfurt, Germany, p. 83 (1999).

Jiang, P., J. Zhang, and L.-S. Fan, "Electrostatic Charge Effects on the Local Solids Distribution in the Upper Dilute Region of Circulating Fluidized Beds," *Circulating Fluidized Bed Technology V*, M. Kwauk and J. Li, eds., Science Press, Beijing, Preprints, DGS14, p. 1 (1996).

Kumar, S. B., D. Mosleman, and M. P. Dudukovic, "Gas-Holdup Measurements in Bubble Columns Using Computed Tomography," *AIChE J.*, **43**, 1414 (1997).

Leung, L. S., R. J. Wiles, and D. J. Nicklin, "Correlation for Predicting Choking Flowrates in Vertical Pneumatic Conveying," *Ind. Eng. Chem. Des. Dev.*, **10**(2), 183 (1971).

Makkawi, Y. T., and P. C. Wright, "Fluidization Regime in a Conventional Fluidized Bed Characterized by Means of Electrical Capacitance Tomography," *Chem. Eng. Sci.*, **57**, 2411 (2002a).

Makkawi, Y. T. and P. C. Wright, "Optimization of Experiment Span and Data Acquisition Rate for Reliable Electrical Capacitance Tomography Measurement in Fluidization Studies—A Case Study," *Meas. Sci. Technol.*, **13**, 1831 (2002b).

Malcus, S., G. Chaplin, and T. Pugsley, "The Hydrodynamic of the High-Density Bottom Zone in a CFB Riser Analyzed by Means of Electrical Capacitance Tomography (ECT)," *Chem. Eng. Sci.*, **55**, 4129 (2000).

Malcus, S., and T. S. Pugsley, "Investigation of the Axial Variation of the CFB Riser Hydrodynamics by Means of Electrical Capacitance Tomography (ECT)," *Fluidization X*, M. Kwauk, J. Li, and W.-C. Yang, eds., Engineering Foundation, New York, p. 763 (2001).

Matsen, J. M., "Mechanisms of Choking and Entrainment," *Powder Technol.*, **32**, 21 (1982).

Neri, A., and D. Gidaspow, "Riser Hydrodynamics: Simulation Using Kinetic Theory," *AIChE J.*, **46**(1), 52 (2000).

Parssinen, J. H., and J. X. Zhu, "Axial and Radial Solids Distribution in a Long and High-Flux CFB Riser," *AIChE J.*, **47**(10), 2197 (2001).

Rowe, P. N., "Experimental Properties of Bubbles," *Fluidization*, J. F. Davidson and D. Harrison, eds., Academic Press, New York, p. 121 (1971).

Satija, S., J. B. Young, and L.-S. Fan, "Pressure Fluctuations and Choking Criterion for Vertical Pneumatic Conveying of Fine Particles," *Powder Technol.*, **43**, 257 (1985).

Seville, J. P. K., J. E. P. Morgan, and R. Clift, "Tomographic Determination of the Voidage Structure of Gas Fluidized Beds in the Jet Region," *Fluidization V*, K. Østergaard and A. Sørensen, eds., Engineering Foundation, New York, p. 87 (1986).

Smolders, K., D. Geldart, and J. Bacyens, "The Physical Models of Cyclone Diplegs in Fluidized Beds," *Chin. J. Chem. Eng.*, **9**(4), 337 (2001).

Takeuchi, H., T. Hirama, T. Chiba, J. Biswas, and L. S. Leung, "A Quantitative Definition and Flow Regime Diagram for Fast Fluidization," *Powder Technol.*, **47**, 195 (1986).

Wang, X. S., and M. J. Rhodes, "On the Use of Choking as a Boundary for Fast Fluidization," *Chem. Eng. Comm.*, **189**(2), 223 (2002).

Warsito, W., and L.-S. Fan, "Measurement of Real-Time Flow Structures in Gas–Liquid and Gas–Liquid–Solid Flow Systems Using Electrical Capacitance Tomography (ECT)," *Chem. Eng. Sci.*, **56**, 6455 (2001a).

Warsito, W., and L.-S. Fan, "Neural Network Based on Multi-Criteria Optimization Image Reconstruction Technique for Imaging Two- and Three-Phase Flow Systems Using Electrical Capacitance Tomography," *Meas. Sci. Technol.*, **12**, 2198 (2001b).

Warsito, W., and L.-S. Fan, "ECT Imaging of Three-Phase Fluidized Bed Based on Three-Phase Capacitance Model," *Chem. Eng. Sci.*, **58**(3–6), 823 (2003a).

Warsito, W., and L.-S. Fan, "3D-ECT velocimetry for Flow Structure Quantification of Gas–Liquid–Solid Fluidized Beds," *Can. J. Chem. Eng.*, in press (2003b).

Warsito, W., M. Ohkawa, N. Kawata, and S. Uchida, "Cross-Sectional Distributions of Gas and Solid Holdups in Slurry Bubble Column Investigated by Ultrasonic Computed Tomography," *Chem. Eng. Sci.*, **54**, 4711 (1999).

Wei, F., H. Lin, Y. Cheng, Z. Wang, and Y. Jin, "Profiles of Particle

Velocity and Solids Fraction in a High-Density riser," *Powder Technol.*, **100**, 183 (1998).
Wiesendorf, V., and J. Werther, "Capacitance Probes for Solids Volume Concentration and Velocity Measurements in Industrial Fluidized Bed Reactors," *Powder Technol.*, **110**, 143 (2000).
Xu, G., K. Nomura, S. Gao, and K. Kato, "More Fundamentals of Dilute Suspension Collapse and Choking for Vertical Conveying Systems," *AIChE J.*, **47**(10), 2177 (2001).
Yang, W. C., "A Mathematical Definition of Choking Phenomenon and a Mathematic Model for Predicting Choking Velocity and Choking Voidage," *AIChE J.*, **21**(5), 1013 (1975).
Yang, W. C., "Criteria for Choking in Vertical Pneumatic Conveying Lines," *Powder Technol.*, **35**, 143 (1983).
Yang, W. C., and S. Liu, "Role of Tomography in Gas/Solids Flow Measurement," *Flow Meas. Instrum.*, **11**, 237 (2000).
Yerushalmi, J., and N. T. Cankurt, "Further Studies of the Regimes of Fluidization," *Powder Technol.*, **24**, 187 (1979).
Yousfi, Y., and G. Gau, "Aérodynamique de l'écoulement vertical de suspensions concentrées gaz–solides: I. Régimes d'écoulement et stabilité aérodynamique," *Chem. Eng. Sci.*, **29**, 1939 (1974).
Zenz, F. A., and D. F. Othmer, *Fluidization and Fluid-Particle Systems*, Reinhold, New York (1960).
Zheng, Y., X. Wan, Z. Qian, E. Wei, and Y. Jin, "Numerical Simulation of the Gas-Particle Turbulent Flow in Riser Reactor Based on k-ϵ-k_p-ϵ_p-Θ Two-Fluid Model," *Chem. Eng. Sci.*, **56**, 6813, (2001).

Manuscript received Mar. 19, 2003, revision received Aug. 25, 2003, and final revision received Dec. 22, 2003.